

On-board impedance diagnostics method of Li-ion traction batteries us- ing pseudo-random binary sequences

Method evaluation and feasibility study of concept

Master of Science Thesis

ZEYANG GENG
CHARALAMPOS SAVVIDIS

Department of Energy and Environment
Division of Electric Power Engineering
CHALMERS UNIVERSITY OF TECHNOLOGY
Göteborg, Sweden 2015

**On-board impedance diagnostics
method of Li-ion traction batteries
using pseudo-random binary sequences**
Method evaluation and feasibility study of concept

ZEYANG GENG
CHARALAMPOS SAVVIDIS

Department of Energy and Environment
Division of Electric Power Engineering
CHALMERS UNIVERSITY OF TECHNOLOGY
Göteborg, Sweden 2015

On-board impedance diagnostics method of Li-ion traction batteries using pseudo-random binary sequences

Method evaluation and feasibility study of concept

ZEYANG GENG

CHARALAMPOS SAVVIDIS

© ZEYANG GENG

CHARALAMPOS SAVVIDIS, 2015.

Department of Energy and Environment

Division of Electric Power Engineering

Chalmers University of Technology

SE-412 96 Göteborg

Sweden

Telephone +46 (0)31-772 1000

Cover:

A cute drawing of an electric bus from Ylva Olofsson.

Chalmers Bibliotek, Reproservice

Göteborg, Sweden 2015

On-board impedance diagnostics method of Li-ion traction batteries using pseudo-random binary sequences

Method evaluation and feasibility study of concept

ZEYANG GENG

CHARALAMPOS SAVVIDIS

Department of Energy and Environment

Division of Electric Power Engineering

Chalmers University of Technology

Abstract

This thesis deals with the on-board impedance measurements of Li-ion batteries on hybrid electric vehicles/electric vehicles by using pseudo-random binary sequences (PRBSs). The impedance of the battery can be related to its state of charge but the accurate impedance measurements are difficult to perform in the vehicles. By using an excitation signal like PRBS, it is possible to extract the impedance information of the battery packs.

Both experiments and simulations are performed with different set-ups to verify the PRBS method. A non-parametric method is used to process the data and extract the impedance measurement. Experiments in the laboratory at different SOC levels and temperatures are made to validate the PRBS method. In the simulations, the noise sensitivity is analyzed.

It is shown that the PRBS method can produce a valid electrochemical impedance spectrum in a limited frequency range, similar to the result from a high accuracy laboratory impedance analyzer. The method is stable at different SOC levels and temperatures. However, the battery impedance at high frequency is difficult to obtain with the PRBS method in the experiments.

A simulation of the excitation signal in the vehicle is performed where the electric motor is used as the load. It shows that it is possible to some extent to use the drive line in a hybrid electric vehicle/electric vehicle to perform an on-board battery impedance measurement.

Index Terms: Li-ion batteries, hybrid electric vehicles, electrochemical impedance spectroscopy, pseudo-random binary sequences, on-board impedance measurement and battery diagnostics.

Acknowledgements

This work has been carried out in cooperation with the Department of Energy and Environment at Chalmers University of Technology and Department of Electrical Engineering at Linköping University. The financial support was given by AB Volvo, Group Trucks Technology, Advanced Technology & Research.

First of all, we would like to thank our examiners Professor Torbjörn Thiringer and Professor Mattias Krysander for their great help during the thesis. Thanks to our supervisor at Volvo, Ylva Olofsson. She considered all the details for us and she was really helpful from all the perspectives. Also thanks to the co-supervisors at Volvo, Jens Groot and Martin West, for all the information they provided us and for their valuable feedback. Thanks to the superior from Linköping University Sergii Voronov.

What is more, thanks to Björn Andersson, Sophie Tintignac, Timofey Maltsev, Mikeal Ohlsson, Zhe Huang, as well as the group manager Jazaer Dawody at GTT AT&R for all the supports and discussions. Also thanks to Stefan Lundberg and Massimo Bongiorno at Chalmers for their help.

Thanks to Mario Salazar Galvez (Volvo Buses Corporation), Espen Helstad (Group Trucks Technology) and Faouzi Al Mouatamid (Volvo Buses Corporation) for giving us the chance to examine our ideas in a vehicle.

Finally, we could not thank enough our families, our friends and especially Jessica Kindström, for their endless support and encouragement throughout the duration of the work.

Zeyang Geng and Charalampos Savvidis
Göteborg, Sweden, 2015

Contents

Abstract	iii
Acknowledgements	v
Contents	vii
1 Introduction	3
1.1 Background	3
1.2 Previous Work	3
1.3 Purpose	5
1.4 Limitation	5
1.5 Outline	5
2 Electric Drive Line and Traction Battery System	7
2.1 Electric Drive Line	7
2.2 Li-ion Battery	8
2.3 Battery Model	8
2.4 Electrochemical Impedance Spectroscopy (EIS)	9
2.5 Battery Diagnostics on Vehicles	10
2.5.1 Inputs to Diagnostic Evaluation	11
2.5.2 Outputs of Diagnostic Evaluation	11
3 System Identification in Li-ion Batteries by Using PRBS	13
3.1 Pseudo-random Binary Sequence (PRBS)	13
3.2 Selection of PRBS Bit Length	15
3.3 Nonparametric System Identification	15
4 Laboratory Set-up	17
4.1 Experiments Set-up	17
4.1.1 Assumption	17
4.1.2 Experiments Procedure	18
4.1.3 Hardware Set-up	18
4.1.4 Standard EIS Measurement	19
4.1.5 PRBS Method Parameters Selection	20
4.2 Simulation Set-up	23
5 Experiments and simulations analysis	25
5.1 Experiment Results	25
5.1.1 Signal Processing	25
5.1.2 EIS Measurement at Different SOC Levels	26
5.1.3 EIS Measurement at Different Temperatures	28
5.1.4 Measurement Limitations	30
5.2 Simulation Results	32
5.2.1 EIS Implementation	32
5.2.2 PRBS Implementation	33

5.2.3	Method Validation	34
6	PRBS Implementation in the Vehicle	41
6.1	Motor Model and Control Algorithm	41
6.1.1	Motor Model	41
6.1.2	Motor Controller	42
6.2	Simulation of the Excitation Signal on the Drive Line	43
6.2.1	Simulation Model of the Drive Line	43
6.2.2	Speed Operation Range	44
6.2.3	Parameters Selection of the PRBS in the Drive Line Simulation	44
6.3	Results and analysis	46
7	Conclusions and Future Work	51
7.1	Conclusions	51
7.2	Future work	51
7.2.1	Improvements for the PRBS method	51
7.2.2	Additional Options for Method Implementation in the Vehicles	52
	References	53
A	Test Conditions	55
A.1	Battery Cell Specification	55
A.2	Layout of the Experiment Set-up	55
B	Simulation Matrix	59

Glossary

BMU Battery Monitoring Unit. 5, 10

CPE Constant Phase Elements. 16

DC Direct Current. 46

EV Electric Vehicle. 8

FOC Field Oriented Control. 41

HEV Hybrid Electric Vehicle. 8

OCV Open Circuit Voltage. 9, 20

PMSM Permanent Magnet Synchronous Motor. 41

PRBS Pseudo-Random Binary Sequence. 13

RMS Root Mean Square. 17, 19, 20

RPM Revolutions Per Minute. 46

SNR Signal to Noise Ratio. 20, 44, 49

SOC State of Charge. 9, 11

SOH State of Health. 9, 11

Chapter 1

Introduction

Ever since the reappearance of the hybrid vehicles in the mid-90s and their bloom in the worldwide market, the usage of Li-ion batteries in the automotive industry has been preferred as means of energy storage for propulsion. One of the most common applications of the Li-ion batteries is in portable computers, and nowadays the automotive industry also turn their attention to them and their advantages. Attractive features include the high energy density and the relatively low self-discharge.

Engineers though, are facing the challenge to make Li-ion batteries and their applications in ways that will be able to predict their life expectancy, degradation and plan production and future actions accordingly due to the unpredictable nature of the ageing mechanism of batteries and how it affects their performances. Especially when the high cost of the automotive application of Li-ion batteries is taken into account, one can understand the importance of being able to use a battery pack of the vehicle to its fullest potential, either if one sees it from the producer's or customer's point of view. Identification of the battery performance, its operations and limits, and how they are affected should be calculated and monitored with the highest accuracy possible in order to avoid expenses in an economic and productive way.

1.1 Background

Automotive companies that offer hybrid or electric variants to their customers usually have their equipment of estimating the battery performance and act based on that. One of the problems is that not always the correct approaches and methods are implemented in the battery monitoring units for the implementation of the battery ageing analysis, thus the accuracy of the measurements will not be of the desired level and factors such as the functionality and reliability may be severely affected. There are after-market companies also that seized the opportunity and offered the growing percentage of hybrid vehicle owners the technology and equipment for service and diagnostics of the battery performance. These systems can perform multiple tasks such as full battery pack service and balancing, de-powering to a safe level after a severe collision, recycling, estimating the battery pack state of health, determining whether it is becoming weak and inefficient. The high cost of owning these systems though, along with the technical knowledge needed to operate them, may constitute these diagnostics systems as difficult to comprehend and therefore not user-friendly enough.

The state of charge (SOC) and the state of health (SOH) are two parameters that affect the battery impedance, but most importantly easy to comprehend when they are used to identify and characterize the battery performance. Especially in the case where the customer of the hybrid vehicle uses the diagnostics system and not an expert or a technician, the interpretation of the measurements is simplified due to the fact that parameters such as the SOC are used extensively in everyday gadgets and appliances such as laptops, mobile phones and more. Based on these parameter measurements, appropriate actions can be planned and performed, either from the manufacturer like replacing the battery pack of the hybrid vehicle or a customer like how to use the battery performance on an everyday basis.

1.2 Previous Work

Explanations, analyses and meanings of concepts such as the EIS and PRBS methods, battery impedance, battery diagnostics and more have been studied in literature such as former Master and Phd student theses

[1] [2], scientific articles, journals and books on batteries and hybrid vehicles for a better comprehension of the subject. Topics, results and conclusions from the aforementioned literature, especially from previous Thesis works that have been performed at Volvo GTT, have been used as reference in the progress and completion of this Master Thesis report.

Previous work also includes algorithms and simulations models that were used in the past and shall be used as examination and reference tools for the conduct of this thesis work. One of the most important simulation models from previous work, not only for its current usability but for functionality examination also, is the Asterics battery model, depicted in Fig 1.1 used previously in [2]. The Asterics model is a complex, yet simple in its use, simulation model of the functionality of a battery. The current and the temperature are used as inputs in the model and it produces results for outputs including the state of charge (SOC) and state of health (SOH).

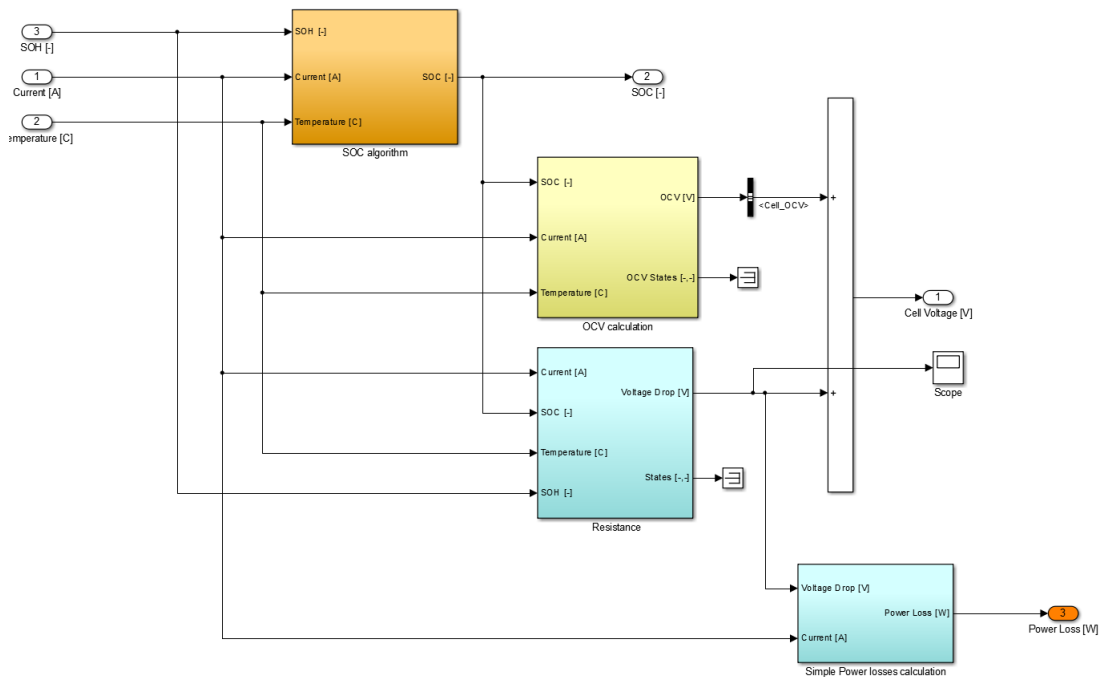


Fig. 1.1 The Asterics Battery reference simulation model.

Several works have been done to investigate the Li-ion battery impedance behavior, especially during the aging [2], [1]. It turns out that the parameters of the battery can be extracted from the electrochemical impedance spectroscopy (EIS), which can be used to characterize the battery state. Most of the EIS analysis are made on cell level using frequency sweep measurement. The EIS analysis of the battery pack on the vehicle level is missing. Nonetheless it is possible to estimate the SOC from the EIS of the batteries on vehicles and the challenges are discussed in [3]. Texas Instruments has been developing an Impedance Track Based Fuel Gauging [4]. It can estimate the remaining capacity for a cell based on its impedance. But it can only be used for single cells in medical equipment application.

A pseudo random binary sequence (PRBS) is a type of signal used in system identification [5]. The PRBS has been used in different areas, including the measurement of power grid impedance [6] and parameters identification of Li-ion batteries [7]. In [8], it shows that the PRBS can be used to measure the EIS of the battery and it can give a better result compared to other signals that are also used for system identification. To be able to measure the battery impedance on-board, the motor can be used as the load to generate the PRBS signal as shown in [3]. This paper also shows a very good example about how to calibrate the measurements.

Other than the PRBS, the system noise can also be used for identification. [9] uses the system noise caused by the telecommunication to measure the battery impedance and it shows good results. In terms of the automotive application, the drive cycle itself can be considered as the system noise. [10] uses the current at the start of the combustion engine as the identification signal in a hybrid electric vehicle. They have built an adapted model which can represent the aging behavior of the battery and the internal resistance can be estimated. But as said in [11], the ohmic resistance and the charge transfer resistance can hardly be

distinguished in this case. [12] uses the extended Kalman filter to observe the impedance of the battery from an urban driving cycle of a hybrid electric vehicle. This method can get the impedance of the battery based on a model with a series of paralleled resistors and capacitors which can approximately get the impedance at very low frequency but cannot describe all the battery behaviors.

What is more, to model the battery in order to represent the EIS, several constant phase elements (CPE), which are nonlinear components, are needed [13], [14]. This increases the difficulty for system identification.

1.3 Purpose

The purpose of this thesis work is to examine, through experiments and simulations, the feasibility and the applicability of an on-board impedance diagnostics method of Li-ion traction batteries using the pseudo-random binary sequence (PRBS) method.

The scope of this thesis is to cover identification of the necessary equipment needed to perform the method on the hybrid vehicle, improvement of the algorithms from the PRBS and EIS method and feasibility analysis of the method. Part of the thesis scope is the creation, with the proper software, of simulation tools to reduce, after validation, the experimental time, effort and cost.

An on-board battery impedance diagnostics system will give the user or the maintenance technician of the hybrid electric vehicle the ability to examine important battery parameters such as the state of health (SOH) and act accordingly.

1.4 Limitation

The aim of the thesis is to focus on the method evaluation. The integration of the impedance measurement to the battery monitoring unit (BMU) algorithm is out of the scope.

This thesis focuses on method validation, which is not limited in one type of Li-ion batteries. So the selection for the electrode material is out of the scope. The cell tested in this thesis is selected by Volvo.

All the experiments are assumed to be at the equilibrium condition of the battery. So the very slow dynamic behavior of the battery is out of the scope of the thesis. More details will be explained in Chapter 4.1.

1.5 Outline

The theoretical part of the thesis is described in Chapter 2, including the drive line in an electric vehicle, the Li-ion battery and its model, the EIS and how to use the PRBS to measure the impedance. The function of the BMU is also introduced. The experiments and simulation set-up are described in Chapter 4. A proposal of the PRBS implementation on the vehicle is presented in Chapter 6, as well as an example of an on-line impedance measurement. The results are discussed in Chapter 5 and finally the conclusion and future work are found in Chapter 7.

Chapter 2

Electric Drive Line and Traction Battery System

The electric drive line constitutes the system that enables an EV or HEV to use electricity from the battery as its fuel and produce motion of the vehicle. The inverter is being supplied with the energy from the battery and with proper control from the BMU and the motor control unit (MCU), it feeds the motor and propulsion is achieved.

2.1 Electric Drive Line

The layout of the electric drive line to be implemented in the thesis report for an electrical vehicle, shown in scheme in Fig 2.1, consists of the components explained in detail in the section to follow.

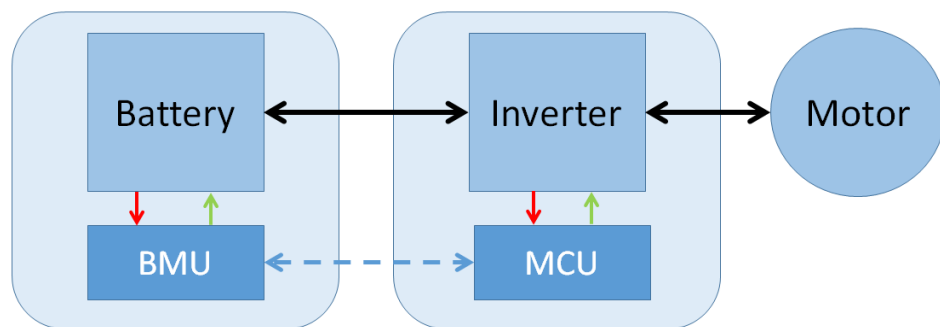


Fig. 2.1 Scheme of the electric drive line in vehicle.

Synchronous electric motors can be found in various sizes and for various applications. The electric machine to be utilized in the case of the thesis work is a synchronous motor. According to [15] this kind of motor is an AC motor in which, at steady state, the rotation of the shaft is synchronized with the frequency of the supply current.

An inverter is an electronic device that transforms direct current to alternating current. The power is supplied by the battery [16].

DC-link capacitors are commonly used on the DC side of the inverter to stabilize the DC side voltage. A significantly sized DC-link capacitor will add unnecessary cost so the manufacturers will choose the smallest capacitor possible. A sufficient capacitor will allow the great majority of the current ripple to flow through the capacitor instead of passing through the battery, thus making the current from the battery to be fairly constant regardless of the switching [17].

The electric energy storage system (battery) is a device that consists of one or more electrochemical cells that convert chemical energy that is stored into electrical energy. A cathode and an anode are contained in each cell and electrolytes allow ions to shift between the opposite terminals thus creating flowing current. Batteries come in various shapes and sizes and can be divided based on their repetition of use in primary or

secondary. A primary battery cell has been designed and manufactured in such a way to be used once and then be discarded after depletion whereas on the other hand, secondary battery cells are the type of cells that can be used repeatedly because of their recharging ability and function [18]. In the conduct of the thesis work all battery cells that are going to be used are secondary. Further details regarding the battery cells that are used, their chemistry and way of work are to follow.

2.2 Li-ion Battery

The Li-ion batteries are widely used in hybrid electric vehicles (HEVs)/electric vehicles (EVs) due to the high power and energy density [1]. There are a variety of types of electrode materials for Li-ion batteries, for example, lithium iron phosphate (LFP), lithium manganese oxide (LMO) and lithium nickel manganese cobalt oxide (NMC). The cell used in this thesis is a LG Chem NMC blend pouch cell and its specification of the cell used is shown in Appendix A.1. This cell has a nominal voltage of 3.75 V and 41 Ah capacity with Mn/NMC cathode and Carbon/Graphite anode.

The battery capacity is usually presented in Ampere-hours (Ah). One way to describe the charge/discharge current is to use the term C-rate. The current is normalized with the battery capacity, for example, 1 C-rate (C/1) means that the current will fully charge/discharge the battery in one hour, 10 C-rate (C/0.1) will fully charge/discharge the battery in 0.1 hour.

The traction battery, which is also called battery pack or energy storage system (ESS), is the main energy source in the EVs. When investigating the possibility and the requirements to implement the EIS measurement on the traction battery, the rated voltage is assumed to be 600 V according to the released data in Volvo 7900 Electric Hybrids.

2.3 Battery Model

The battery model that is implemented and used for the simulations in the line of the thesis work takes the current and the temperature as inputs and calculates outputs such as the voltage and the SOC. Data taken from the simulations (simout), as shown in Fig 2.2, are used in the implemented algorithms for the further examination of the EIS and PRBS methods.

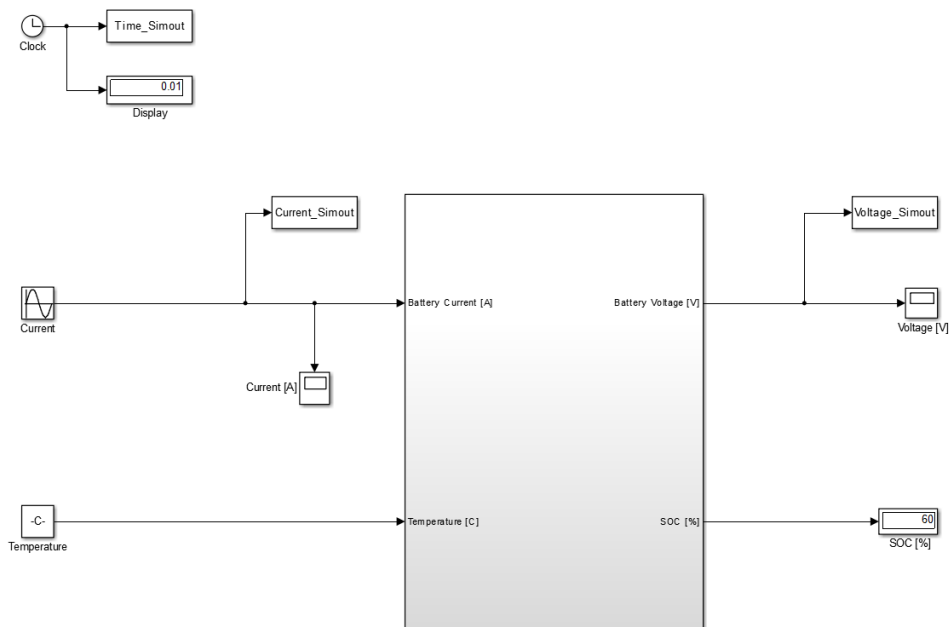


Fig. 2.2 Battery model simulation

The parameters to be used for all the calculations needed in the battery model such as the battery nominal capacity, the initial hysteresis, scalars, factors and more, are defined from the start in a Matlab

workspace file and loaded for use when called. The most important of those parameters and the effect of which is more in line with the scope of the thesis are defined and altered accordingly for each simulation in the beginning of the controlling algorithm of the implementation. Such parameters are the initial SOC and SOH, the temperature and more.

The state of charge is being calculated by having the initial SOC, as defined by the user, and then with the use of scaling functions, SIMULINK blocks and mathematical equations, the final value of the SOC is being calculated for the experimental simulation.

The voltage is being calculated through two main components, one from the OCV calculation and one from the resistance of the battery. The OCV calculation is being done with the use of proper blocks and equations connecting all the essential parameters along with a more complex function, implemented for the calculation of the hysteresis of the battery, with hysteresis being the time-based dependence that an output has on the input it is subjected to currently and from the past [19].

The resistance on the other hand is being implemented by calculating the double layer capacitance, the charge transfer resistance, the Warburg capacitance, the polarization resistance and the ohmic resistance. From the above, the charge transfer, polarization and ohmic voltage drops are calculated and their sum is the total voltage drop. Equally, the total voltage drop along with the open circuit voltage are the components to be summed for the calculation of the voltage output of the battery cell. For the voltage of the battery pack, the number of cells in series or parallel configuration must be taken into consideration and calculated accordingly.

The battery model, as implemented, offers the option also to the user to operate the model as a battery cell or a battery pack. The number of cells that will constitute the battery pack along with the configuration on which they are going to be placed can be defined and changed for each simulation, depending on what is examined. When a parallel configuration is used, the voltage is the same through all the cells and the current is the sum of the currents of each individual cell.

In contrary, in series configuration the current is the one that is the same throughout the circuit and the voltage is calculated as the sum of all voltages from each individual cell [20].

The configuration depends on the application the battery pack will be used, it is common also to meet combinations of these configurations in a single circuit system, so there is the possibility to perform the same in the battery model. What it can be said, and it is explained by the fact that in serial configuration the voltage is constantly added up and subsequently increased, that the layout to be preferred is based on the needs and expectations one expects from the battery pack. If high voltage is the demand then a serial configuration must be preferred whereas if high current is to be created then the recommended configuration is the parallel.

2.4 Electrochemical Impedance Spectroscopy (EIS)

EIS is one of the most common experimental methods for the characterization of electrochemical systems and one that is used extensively in battery cell research [21]. In this method, the impedance of a system over a range of frequencies is being measured, energy storage and dissipation properties are revealed by the frequency response.

Advantages that have made the method of EIS extensively used in a wide variety of scientific areas include measurements that are not being intrusive, impedance parameters such as the ohmic and charge-transfer resistance can be estimated from an experiment, relatively simple method so procedural simulation constitutes a viable and usable option, high precision in the measurements because they can be averaged over a long time to improve the signal-to-noise ratio [22].

A way to depict the EIS method and afterwards interpret and utilize its results is through a Nyquist plot. For a range of frequencies, the real and imaginary parts of the impedance constitute the axis of the plot. From the Nyquist plot, the values of important parameters such as the ohmic and charge transfer resistances can be identified, as seen in Fig 2.3. The ohmic resistance is the intersection with the real axis of the impedance curve in the Nyquist plot whereas the charge transfer resistance is the real impedance approximately at the local minima of the impedance curve in the Nyquist plot [2]. Another important parameter to be taken into account is the double layer effect, which is the formation of two layers of opposite polarity at the interface between electrode and electrolyte. This phenomenon occurs when an electronic conductor is brought in contact with a solid or liquid ionic conductor [23].

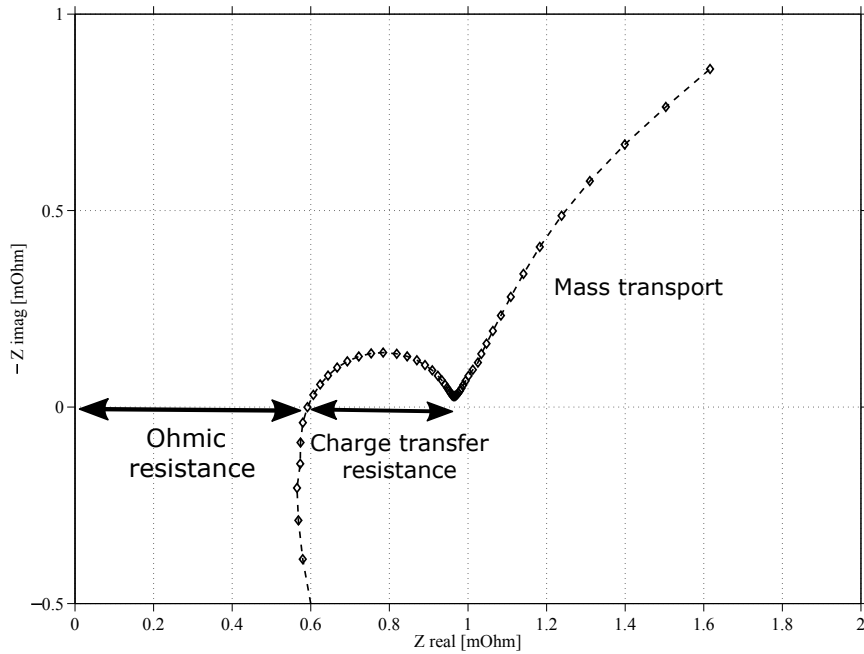


Fig. 2.3 Ohmic and Charge Transfer resistance in the Nyquist plot.

The importance of these parameters lies on the position they have on an electric circuit. As depicted below in Fig 2.4, both the ohmic resistance R_{ohm} and the charge transfer resistance R_{ct} constitute important parts of the circuit along with the voltage supply and more.

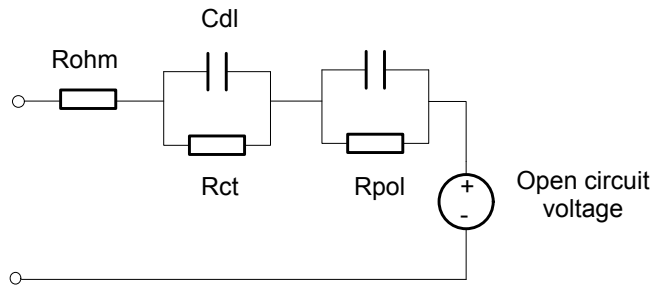


Fig. 2.4 Simplified battery model.

2.5 Battery Diagnostics on Vehicles

In order to monitor and control the battery operation a battery monitoring unit (BMU) is used. By operating the battery cell or pack at certain conditions and with the aid of the BMU, the required states that are to be calculated can be found. The BMU generally takes parameters such as the battery current, voltage and the operating temperature into account and gives results regarding the impedance, the SOC and the SOH of the battery.

A battery management system is an electronic system that can manage a battery cell or pack and perform operations such as protecting the battery from operating outside its safe operational area, monitor its states, calculate and report secondary data etc [24]. In particular the monitoring unit detects the battery's voltage, current and temperature as well as other parameters and produces the required data, as depicted in Fig 2.5.

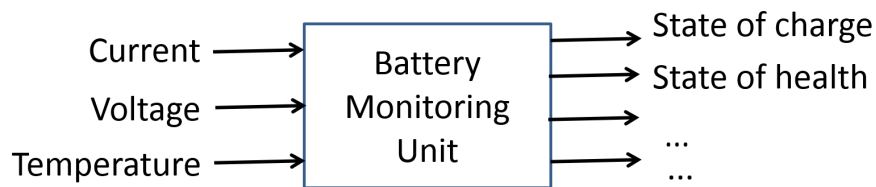


Fig. 2.5 Battery monitoring unit scheme

For Li-ion batteries it is necessary to measure the voltage of each cell, then these analog voltage data are converted to a digital form and if it is detected that a cell is operating at a higher voltage it makes it discharge, a procedure known as balancing of the cell. [25].

2.5.1 Inputs to Diagnostic Evaluation

The battery monitoring unit takes the current and voltage, as well as the temperature of the battery as the inputs. According to [26] if a device, the battery in this particular case, is exposed to operation outside the limits of its temperature range, it will age faster and the risk of failure will be increased.. For Li-on batteries the charging temperature limits are different than the operational, this means that even though it will function the battery charging will not be as effective in all of the range. In particular, a temperature range between $25\text{ }^{\circ}\text{C}$ and $45\text{ }^{\circ}\text{C}$ allows for an optimized fast-charging whereas low temperature charging (0 to $5\text{ }^{\circ}\text{C}$) is possible but the charge current should be reduced, high temperature charging (above $45\text{ }^{\circ}\text{C}$) is not recommended due to the fact that it degrades the battery performance [27].

2.5.2 Outputs of Diagnostic Evaluation

Electrical impedance can be quantified as the complex ratio of the voltage to the current in an AC circuit and it is the extension of the resistance concept in AC circuits. When the impedance is caused by the inductance and the capacitance it forms its imaginary part whereas the real part is formed by the resistance [28].

State of charge (SOC) is the charge that the battery currently has for any operation and it is measured in percentage of the fully charged capacity [29].

State of health (SOH) is a measurement that shows the amount of “life“ that is remaining in the battery and it is therefore depicted in a percentage of the total original capacity of the battery [30]. Typically, a battery’s SOH will be 100 per cent at the time of manufacturing and will decrease over time and use. Batteries though, with capacity under 80 per cent are considered depleted and therefore no more useful on automotive application.

Chapter 3

System Identification in Li-ion Batteries by Using PRBS

For the purpose of battery impedance characterization, the battery can be considered as a linear system. The white noise can be used to identify a system since it contains the information at whole frequency range. However, an ideal white noise doesn't exist in reality so other excitation signals need to be investigated. The PRBS signal is selected in this work for system identification.

3.1 Pseudo-random Binary Sequence (PRBS)

The PRBS signal is a band-limited white noise, which can be used to identify a linear system in a certain frequency range. A PRBS signal switches between two states. More details about how to design a PRBS signal and how to implement it in the computers are well explained in [5]. An example of an 8-bits PRBS signal is given here.

One way to generate the PRBS is to use linear feedback shift registers (LFSRs) [31]. (The corresponding Simulink functions in MATLAB are the *Unit Delay* and *XOR Logical Operator*). An 8-bit PRBS generator is shown in Fig. 3.1.

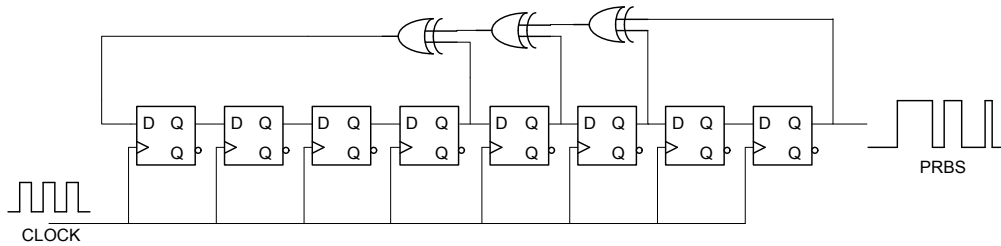


Fig. 3.1 An 8-bit PRBS generator example

For a n-bit PRBS, the total number of possible states N is

$$N = 2^n - 1 \quad (3.1)$$

For an 8-bit PRBS, the registers can have 255 different states. The PRBS which can go through all the states is called maximum length sequence, which is most of the cases when it is designed for system identification. The PRBS signal will repeat every N states so it is a periodic signal. As the bit length of the PRBS is increasing, it will take a longer time to go through every state. The whole testing time will increase exponential with the number of bits.

Another important factor for a PRBS signal is the clock frequency f_c , which is the shifting frequency for the registers. The delay time T_c in the delay unit in Fig. 3.1 is set to be

$$T_c = \frac{1}{f_c}. \quad (3.2)$$

For example, when $f_c = 10 \text{ Hz}$ and the all the initial states in the register are 1, the 8-bit PRBS is shown in Fig. 3.2.

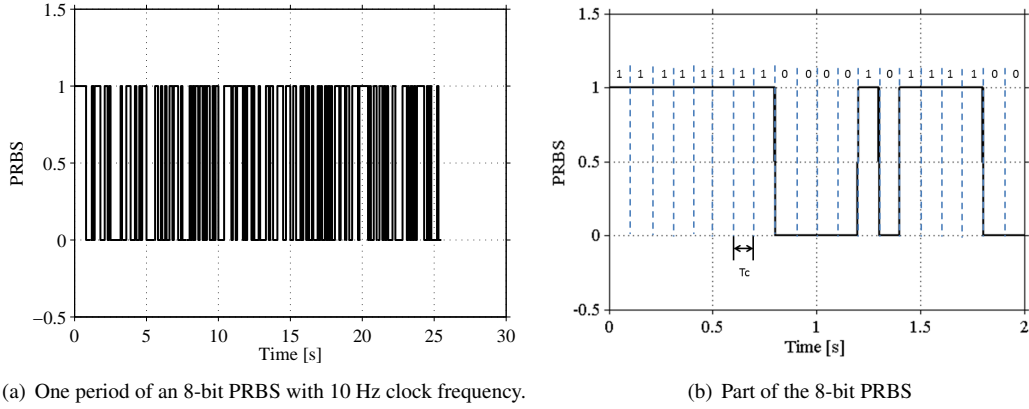


Fig. 3.2 An example of an 8-bits PRBS with 10 Hz clock frequency.

The advantage of the PRBS is that it is not correlated with itself within one period. The auto-correlation function of the 8-bit PRBS is shown in Fig. 3.3(a). This PRBS repeats for three periods and it can be seen that it is only autocorrelated once after one period. Thanks to this pseudo-random characteristic, the PRBS contains signals in a wide frequency range.

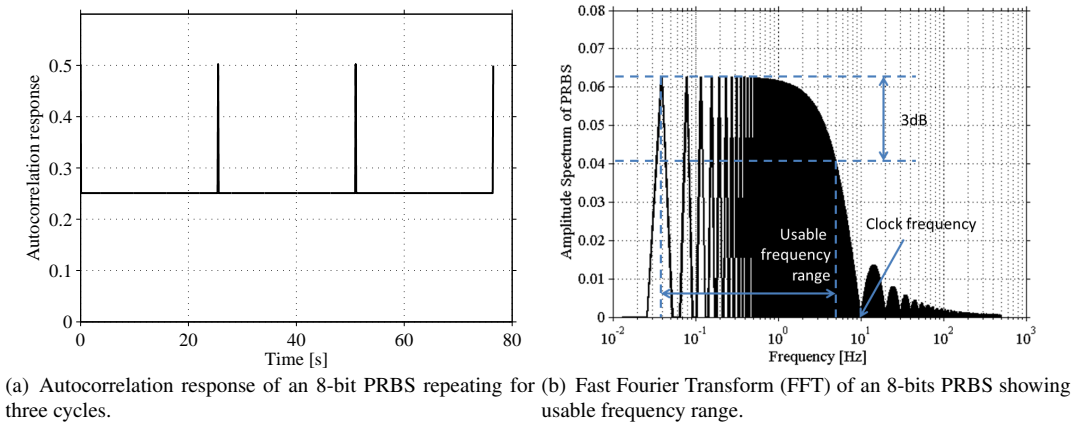


Fig. 3.3 The autocorrelation response and frequency domain characteristic of the previous PRBS.

The number of bits n and the clock frequency f_c determine the usable frequency range of a PRBS, which can be studied by using the Fourier Transform, as shown in Fig. 3.3(b). The usable range is defined by the 3-dB bandwidth (it is called the half power bandwidth) [5]. The minimum frequency f_{min} , which is the first frequency point after the DC, is

$$f_{min} = \frac{f_c}{N} \quad (3.3)$$

and the maximum frequency f_{max} which is when the amplitude of the signal decreases to 3 dB of its peak value, is

$$f_{max} = \frac{f_c}{3} \quad (3.4)$$

according to [32]. Ideally, a PRBS signal only contains the information at the certain frequency points. The frequency step is

$$\Delta f = f_{min} \quad (3.5)$$

Therefore, a PRBS contains usable information at $f_{min} : \Delta f : f_{max}$.

3.2 Selection of PRBS Bit Length

In the battery reactions, different phenomenons have different time constants. The double-layer effect can reflect the SOC of the battery as shown in Fig. 3.4. So the target of the PRBS measurement is to capture the double-layer effect.

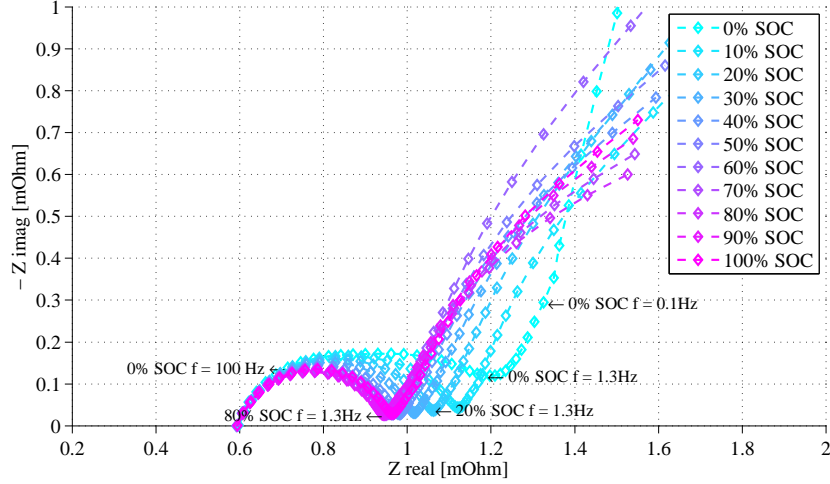


Fig. 3.4 EIS at different SOC levels for a LG Chem 41 Ah cell. Testing conditions: beginning of life, 22°C.

The time constant of the double-layer effect depends on the chemistry of the battery. For most of the batteries, the time constant is in the range of milliseconds to some seconds [33]. For the cell used in this thesis, the time constant is shown in Fig. 3.4. As it can be seen, the point that can be used to identify the charge transfer resistance (SOC dependent point) is located around 1 Hz. Therefore, the usable frequency of the designed PRBS needs to cover around 1 Hz for the selected cell type. The lowest frequency is selected to be 0.15 Hz to capture the curve clearly.

A comparison is made among different bit length of PRBSs in Table 3.1. The consumed time is calculated for five cycles as an example. A higher clock frequency will reduce the testing time and cover a wider frequency range but it will also introduce difficulties for the system identification which will be explained in Chapter 5.1.4. In this thesis, an 8-bit PRBS is selected as a balance between the clock frequency and the testing time.

Table 3.1: Comparison of different bit length of PRBS (The desired lowest frequency is 0.15 Hz).

PRBS bits	Frequency range	Clock frequency	Testing time
6-bit	0.15 Hz : 0.15 Hz : 3.33 Hz	10 Hz	127.50 s
8-bit	0.15 Hz : 0.15 Hz : 13.33 Hz	40 Hz	31.88 s
10-bit	0.15 Hz : 0.15 Hz : 53.33 Hz	160 Hz	7.97 s
12-bit	0.15 Hz : 0.15 Hz : 213.33 Hz	640 Hz	1.99 s
14-bit	0.15 Hz : 0.15 Hz : 853.33 Hz	2560 Hz	0.50 s

3.3 Nonparametric System Identification

A single input single output (SISO) model of a linear time invariant (LTI) system is presented in Fig 3.5. The transfer function is a main tool to describe the behavior of a LTI system [34]. The basic idea of the transfer function is to look at the system from its frequency response.

If the input current is periodic, it can be decomposed into the sum of a series sinusoidal waves and cosine waves,



Fig. 3.5 A general SISO system.

$$u(t) = \sum_{k=0}^{\infty} a_k \sin(k\omega t) + b_k \cos(k\omega t), \quad (3.6)$$

where ω is the fundamental frequency of the input. Each term of the input will cause a corresponding output with different amplitude and phase [34]. The gain and the phase shift at different frequency represent the transfer function of the system.

For each frequency $k\omega$,

$$Y(k) = G(i\theta)U(k) = Me^{i\theta}U(k), \quad (3.7)$$

$$e^{i\theta} = \cos \theta + i \sin \theta \quad (3.8)$$

where $U(k)$ and $Y(k)$ are the input and output at the frequency $k\omega$, $Z = Me^{i\theta}$ is the polar form of a complex number with the gain M and the phase shift θ .

In this thesis, the battery is considered as a SISO model. The input signal $u(t)$ is the current and the output signal $y(t)$ is the voltage. Therefore, the impedance of the battery is the transfer function of the system. The current input can be expressed in (3.6) and a current input at $k\omega$ frequency can cause a voltage output also at $k\omega$ frequency with certain gain and phase shift,

$$U(k) = ZI(k) = |Z|e^{i\theta_z} I(k) \quad (3.9)$$

where $I(k)$ and $U(k)$ are the input current and output voltage at the frequency $k\omega$, $|Z|$ and θ_z are the gain and the phase of the impedance at this frequency. Therefore,

$$\begin{cases} |Z(k)| = \frac{|U(k)|}{|I(k)|} \\ \theta_z(k) = \theta_u(k) - \theta_i(k) \end{cases} \quad (3.10)$$

The impedance could be presented in form

$$Z(k)_{real} = |Z(k)| \sin \theta_z(k), \quad Z(k)_{imag} = |Z(k)| \cos \theta_z(k) \quad (3.11)$$

When a PRBS input current is applied to the system, the valid points are located at $f_{min} : \Delta f : f_{max}$ as discussed in the previous section. This nonparametric identification method simply takes the input and output signals without any fitting and it can be used in any system. It is straight forward but on the other hands it is sensitive to the noise and the nonlinear distortion.

The parametric identification is more robust to the noise and the nonlinear distortion but it requires a model to be able the identify the signals. As mentioned in [13] and [14], to model the battery accurately, several nonlinear constant phase components (CPEs) are needed. So it is very difficult to model the battery with a LTI system to perform the parametric identification. What is more, the purpose of the thesis is to investigate a method that can be used on-board by utilizing current processors on the vehicle without additional equipment. The parametric identification increases the computation load and it makes the implementation on-board even more difficult.

Compared to the parametric identification, the nonparametric one is more simple and it can give sufficient results in the laboratory environment. And almost all the previous work related to PRBS identification are performed with nonparametric identifications. The parametric identification is only used with some adapted models which only present limited information. Therefore, the nonparametric identification is used in this thesis work.

Chapter 4

Laboratory Set-up

Both the experiments set-up and the simulation set-up for the EIS will be explained in this chapter. For the experiments, the assumption, testing procedure, hardware set-up and the parameter selection are explained and analyzed. The simulation model and its algorithms are also introduced.

4.1 Experiments Set-up

This section presents the experiments assumption, the equipment and their connections, as well as the parameters that to be selected. The experiment results in Chapter 5 are based on this set-up. More information about the equipments can be found in Appendix A.2.

4.1.1 Assumption

In the experiments, all the cells are assumed to be at the equilibrium condition. The reason is that the impedance of the battery keeps changing after charge/discharge until reaching the equilibrium state. A test is made to show this difference. In this test, a 41 Ah cell is charged from 20% SOC to 50% SOC at 0.5 C-rate. The EIS is measured at three different time points, just after the charging, 15 minutes after the charging and 60 minutes after the charging. To compare the different effects of charging and discharging, the same cell is discharged from 80% SOC to 50% SOC and the EIS is measured in the same way. The EIS after the charging measurement is using a frequency sweep with sinusoidal waves. The root mean square (RMS) value of the signal is 10 mV to avoid additional disturbances to the battery state. The result is shown in Fig. 4.1.

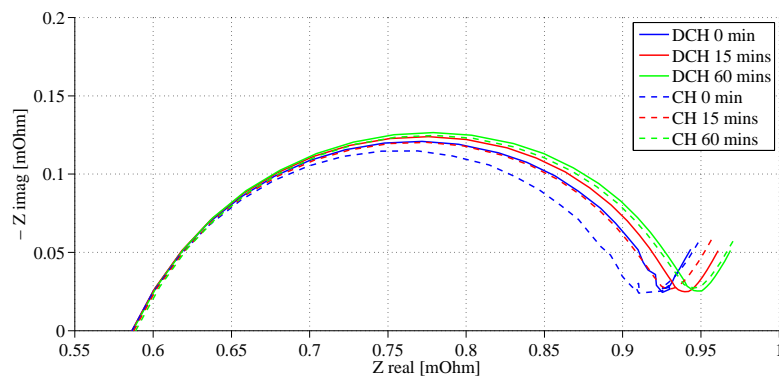


Fig. 4.1 EIS measurement at 0 mins, 15 mins and 60 mins after 36 mins charging from 50% SOC to 80% SOC at 0.5 C-rate.

As it can be seen, the EIS varies at different time instants. The mechanism of the battery dynamic behavior is described in [33]. Further explanations are out of the scope of this thesis. What is more, the PRBS input current signal is selected to be 10 A in the following tests to get good results based on the

evaluation described in the following section. So other than the charge/discharge, the PRBS measurement itself also causes the change of the battery state and it can not be neglected.

4.1.2 Experiments Procedure

To make the above assumption valid, the experiments in the thesis follow the procedure shown in Fig. 4.2 and 4.3. For the experiments at different SOC levels, it is not necessary to wait for 24 hours. The reason to have a 24 hours interval is that the SOC level test cannot be finished within one work day even with shorter interval. Since the tests are performed manually, it will be interrupted by an overnight interval. Therefore, waiting for 24 hours between each SOC level can keep the interval constant. With an automated testing equipment the test interval can be shorter.

As it can be seen, each PRBS measurement is followed by a 15 mins interval before a standard EIS measurement. This is because that the PRBS measurement changes the state of the cell due to its high current. If a standard EIS measurement is taken just after the PRBS measurement, a difference can be noticed, similar to Fig. 4.1.

In the experiments at different temperatures, the battery has a rest time of three hours. This is defined as the rest period needed for the battery cell to reach a steady temperature.

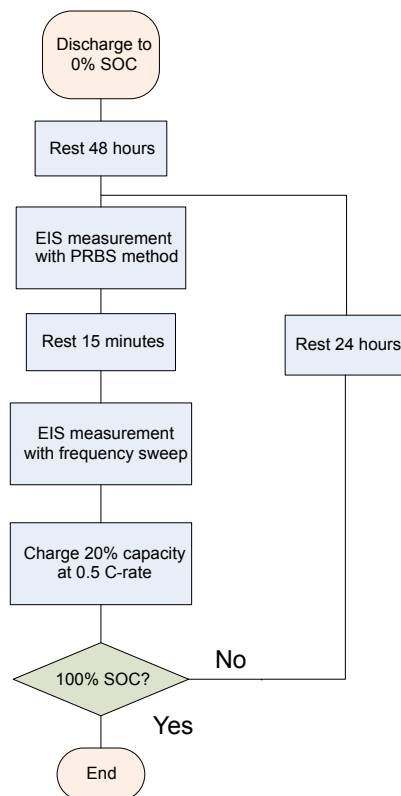


Fig. 4.2 Experiments procedure for the EIS measurement at different SOC levels.

4.1.3 Hardware Set-up

The instruments that are used in the experiments are listed in Table 4.1. The GAMRY Reference 3000 is a hardware which is developed to measure the EIS of a test object with high accuracy. Therefore, the EIS measurement from the GAMRY is used as a reference to verify the PRBS method. The GAMRY can only be operated in a limited voltage and current range (± 1.5 A at ± 30 V or ± 3 A at ± 15 V), so a booster with ± 30 A output current is used to increase the output power. The VFP 600 is a software-based front panel for the GAMRY instrument. With the help of the VFP 600, the GAMRY can be used to generate a defined signal, which is a PRBS signal in this thesis work. Therefore, the GAMRY can perform both the standard EIS measurement and the PRBS method.

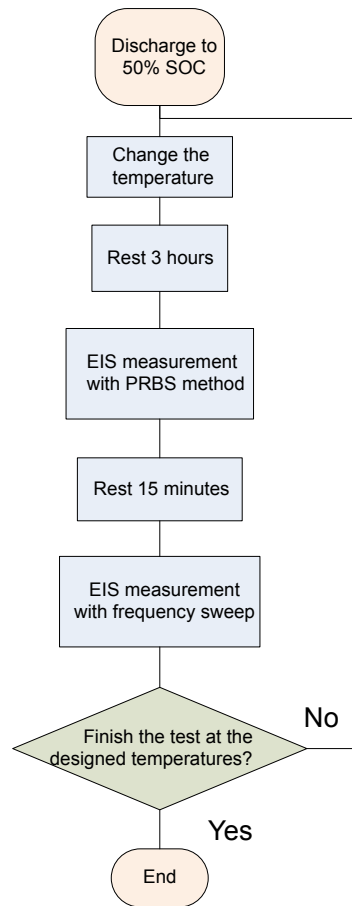


Fig. 4.3 Experiments procedure for the EIS measurement at different temperatures.

Table 4.1: Experiment Instruments used in the laboratory.

	Instrument	Function
1	GAMRY Reference 3000	Power source and standard EIS reference
2	GAMRY Booster	Increase the output power of the GAMRY Reference 3000
3	DL750 ScopeCorder	Data acquisition recorder
4	Current Probe Model PR30	AC/DC current probe
5	Climate Chamber	Control the temperature
6	Computer	Control the GAMRY Reference 3000 with the VFP 600

In the experiments, the GAMRY is mainly used as the power source. It can be used to log the data but the maximum sampling frequency is 4 kHz. It is sufficient for the low clock frequency PRBS according to the following results. However, to be able to capture some signals with high enough sampling frequency, an additional data acquisition set-up is needed. The DL750 ScopeCorder from Yokogawa Test & Measurement is a high speed oscilloscope and traditional data acquisition recorder. The Current Probe Model PR30 from LEM is a high bandwidth AC/DC current probe and it is suitable for this experiment. The layout of the hardware set-up is shown in Appendix A.2.

4.1.4 Standard EIS Measurement

One common way to measure the EIS is by using frequency sweep so that the impedance at each frequency can be measurement individually. In most of the applications, the RMS value of the frequency sweep is 10 mV without offset.

Even though the battery can be considered as a linear system in this thesis, this is only valid within a short time under certain conditions. Over a long period and under different conditions, the battery is a complicated non-linear system and the EIS is slightly affected by the current amplitude [21]. To examine the PRBS method, the frequency sweep is designed to be as similar to the PRBS signal as possible. So in

this thesis if it is not specified the the RMS value of the frequency sweep is the same as the PRBS current instead of 10 mV.

4.1.5 PRBS Method Parameters Selection

To design a PRBS experiment, several parameters need to be selected. The impacts and limitations of each setting will be discussed in this section.

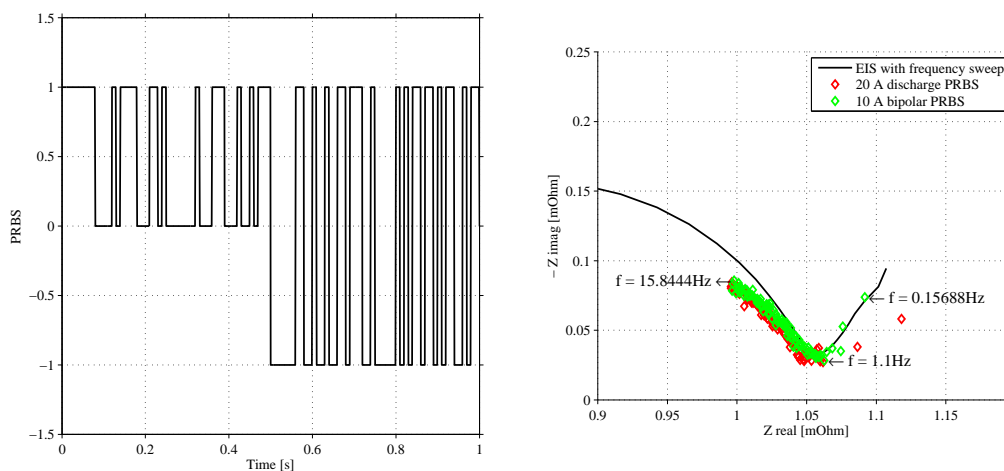
Current amplitude

A high current input can improve the signal to noise ratio (SNR). The applied current needs to be high enough to cause significant voltage variations, which can be easily detected by the voltage sensors. For the selected cell, a 10 A current can cause a 10 mV voltage change. Since the lab environment has a very low noise level, the SNR is high enough with a 10 A current signal. If the experiment needs to be performed in a noisy environment, a higher current can improve the results.

The impedance of the battery will be slightly different under the testing current with different amplitude. To validate the PRBS method, the EIS in the standard measurement method need to be measured with the same amplitude current. Therefore, the RMS value of the sinusoidal wave in the frequency sweep is set to be 10 A.

Sign of signal

The PRBS is a sequence changing between two states. When the two states have the same sign, for example from 0 to 1, the sequence is called unipolar. If the two states have different sign, for example from -1 to 1, it is called bipolar. As shown in Fig. 4.4(a), the former part of the signal is unipolar while the later part is bipolar.



(a) An example of unipolar PRBS and bipolar PRBS.

(b) EIS measurement effects of unipolar PRBS and bipolar PRBS. The phase shift at low frequency with unipolar PRBS is due to the OCV shift.

Fig. 4.4 Comparison of unipolar and bipolar PRBS.

A unipolar (charge or discharge) signal will cause the SOC and OCV to change during the experiment. The SOC changes affect the parameters to be identified. And the OCV changes cause a linear trend in the measurement, which can be considered as a low frequency disturbance. The result is shown in Fig. 4.4(b). As can be seen that by using an unipolar signal, the impedance below 1 Hz is shifted. The shifting at frequency higher than 1 Hz is due to the sampling frequency which will be discussed later. This influence can be decreased by applying lower current input and shorter testing time.

A bipolar signal will not affect the SOC during the experiments. However it requires that the equipment can generate a bipolar signal. A bipolar signal is used in the experiment since the GAMRY Reference 3000 can generate a bipolar signal.

Rise time and slew rate of the current steps

The PRBS is a square wave and a good PRBS signal needs to have clear current steps, which means a fast rise time and no overshoot. There are five options in the VFP600 setting: Fastest, Fast, Normal, Medium and Slow. The comparison of current steps of the options Fast, Normal and Medium is shown in Fig. 4.5. The sampling frequency of the current step is 5 Msps.

Table 4.2: Rise time and slew rate of the current steps in different mode.

	Rise Time	Slew Rate
Fast	4 μs	3.84 A/ μs
Normal	70 μs	1.20 A/ μs
Medium	490 μs	0.16 A/ μs

The rise time is the time taken by the signal to change between 10% and 90% of the step height. The slew rate is the maximum rate of change of the current per unit of time. The two parameters are calculated from the measurement, shown in Table 4.2. The fast rise time can contribute to a sharp current step but on the other hand the high slew rate will cause voltage spike with the inductance in the system. Therefore, the Normal mode is selected in the following experiments as a balance.

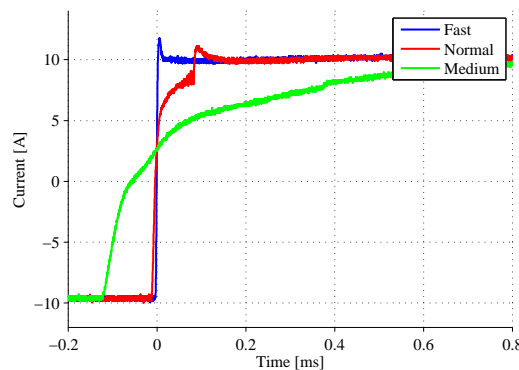


Fig. 4.5 The current steps of different modes in the VFP 600 settings with 5 Msps sampling frequency.

Cycle number

The PRBS is a periodic signal and it requires integer amount of cycles when the data is analyzed with Fast Fourier Transform (FFT). More cycles can make the data more concentrated at the frequency points in the frequency domain, but more cycles will take a longer time and it will also produce a large amount of data to store and to process. The cycle number is selected to be five in this work, which is chosen to balance between accuracy and the data size.

Measurement bandwidth

As said before, the signals in the experiments are measured by two different data acquisitions, one is the GAMRY internal logging, the other is the oscilloscope with a current probe. It is noticed that there is a difference between the logged data, as shown in Fig. 4.6. The sampling frequency of the GAMRY is 4 kps and the sampling frequency of the oscilloscope is 5 kps/10 kps. The oscilloscope is set to be full bandwidth. It is assumed that the measurement from the oscilloscope can present the real signal since the distortions caused by the oscilloscope measurement can be neglected at the frequency range of mega hertz. From the measurement from the oscilloscope at 10 kps, spikes can be noticed. The spikes are existing in the signal but not caused by the measurement. The reason of the spikes will be explained in Chapter 5.1.4.

It shows that there is a low-pass filter or a similar filter inside the GAMRY measurement. The detailed information is not available from the data sheet. However, the GAMRY measurements give better results compared to the oscilloscope measurements. Therefore, the measurement from the GAMRY is selected for the method validation other than the oscilloscope and the results shown in Chapter 5 are from the GAMRY

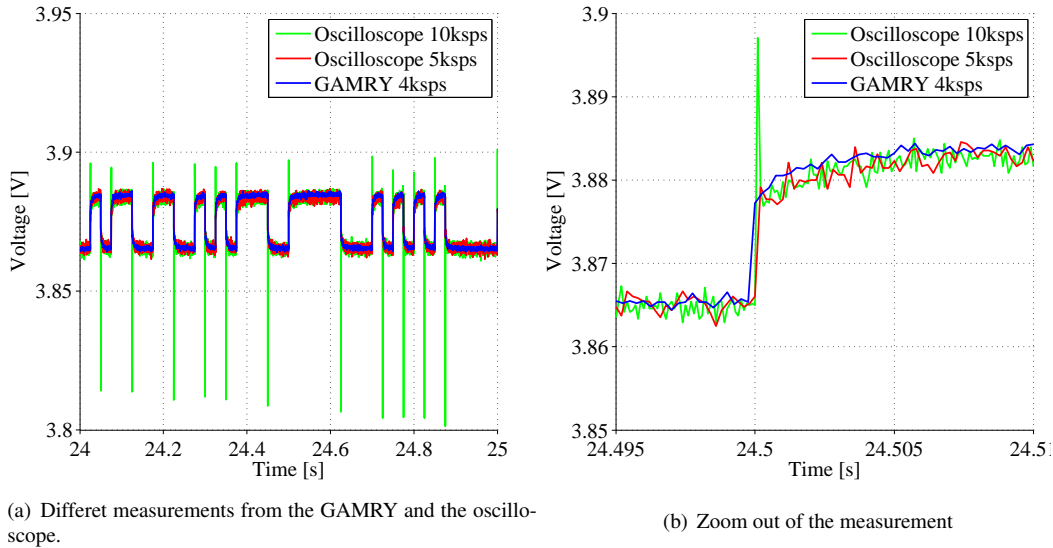


Fig. 4.6 Different measurements from the GAMRY and the oscilloscope. The sampling frequency of the GAMRY is 4 kps and the sampling frequency of the oscilloscope is 5 kps/10 kps.

measurements. The oscilloscope measurements are mainly used to analysis the data since it can sample much faster than the GAMRY. In theory, the measurements from the oscilloscope can achieve the same result by applying some digital filters. Due to the time limitation, this is not implemented in this thesis.

Measurement resolution

In normal commercial data acquisition systems, 12-bit or 16-bit analog to digital converters (ADCs) are widely used. A higher bit ADC gives a higher resolution but adds additional cost. For the selected cell, the voltage range is 3.0 V to 4.15 V and the voltage change caused by a 10 A PRBS current is 10 mV. The 12-bit ADC shows a poor result while the 16-bit ADC performs better, as shown in Fig. 4.7. Therefore, in other measurements from the oscilloscope the 16-bit ADC is always used.

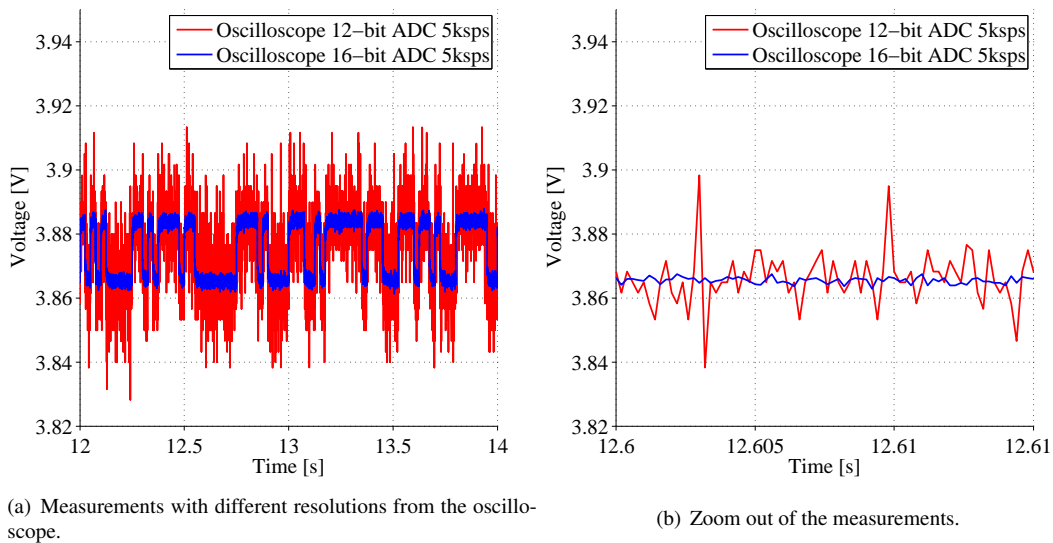


Fig. 4.7 Measurements from 12-bit and 16-bit ADCs from the oscilloscope.

This should be taken care of when the measurement is performed on the vehicle level. Assume a data acquisition with 1000 V measurement range and a 16-bit analog to digital converter (ADC) is used to

measure voltage on the battery pack on the vehicle whose rated voltage is around 600 V, the resolution is

$$V_{resolution} = \frac{V_{full-scale}}{2^{16} - 1} > \frac{1000 V}{65535} = 15.2590 mV. \quad (4.1)$$

Whether this resolution is sufficient depends on the impedance of the battery pack and the input current signal.

Sampling frequency

According to the Nyquist-Shannon sampling theorem [35], if a signal contains no higher frequency than f , a sufficient sampling frequency is $2f$. Equivalently, a sampling frequency f_s can properly determine the characteristics of a signal with a bandwidth of $f_s/2$. However, in reality, the sampling frequency needs to be much higher than the Nyquist sampling frequency, maybe more than 10 times to achieve good results. A low sampling frequency will cause phase shift and possible aliasing signal [35]. The clock frequency of the PRBS is 40 Hz.

The phase shift caused by the sampling frequency can be seen in Fig. 4.8.

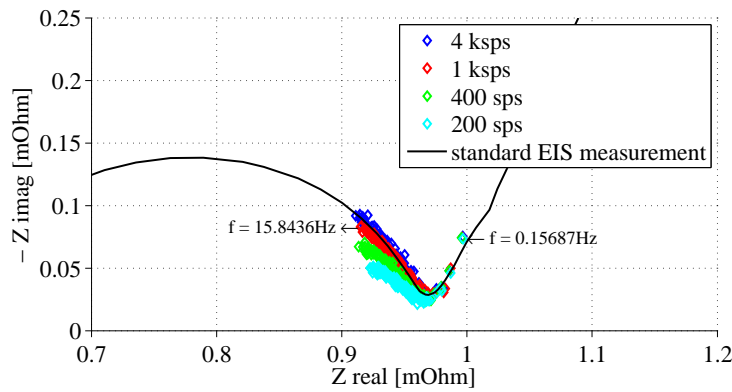


Fig. 4.8 EIS measurement with different sampling frequency showing the phase shift. Testing conditions: 50% SOC, 22°C.

The phase shift can be analyzed easier in the bode plot in Fig. 4.9. As can be seen that with the sampling frequency reducing, the amplitude of the impedance can still be identified properly but the phase starts to shift. The phase shift is larger at the higher frequency range. Both of Fig. 4.8 and 4.9 are from the GAMRY measurement.

The parameters selected in the PRBS method are summarized in Table 4.3.

Table 4.3: Summary of the parameters used in the experiments for the method validation.

Parameter	Value
Current amplitude	10 A
Sign of signal	Bipolar
Rise time and slew rate of current steps	70 μ s and 1.20 A/ μ s (Normal mode in GAMRY)
Cycle number	5
Measurement bandwidth	GAMRY internal filter
Measurement resolution	GAMRY internal setting
Sampling frequency	4 kHz

4.2 Simulation Set-up

As in the battery model implementation, engineering software such as Matlab and Simulink has been used for the creation of simulation algorithms and models that will aid the progress, goals and completion of this Master Thesis. The aim is to simulate as accurately as possible the results from the lab experiments. It is also essential to do it in the simplest and most user-friendly way possible, run the experiments, validate data and compare results.

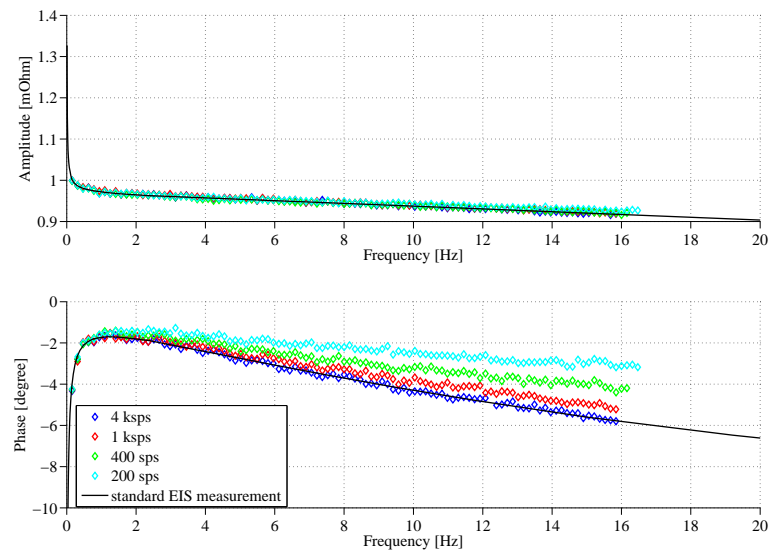


Fig. 4.9 EIS measurement with different sampling frequency in bode plot showing the phase shift. Testing conditions: 50% SOC, 22°C.

The simulation of both the EIS and PRBS signals on a battery cell and on the electric drive line serves the purpose of method validation. The EIS method is used as a reference and the findings of the PRBS are compared to those of the EIS reference. The validation can save a lot of time, especially in cases in which electrical components are simulated through various parameters and variables. The simulation model aims at speeding up the procedures of examining all the required experiments for the thesis work and for any future work on the subject.

For both EIS and PRBS battery models, the EIS and the PRBS are the current input in the battery, and a suitable algorithm has been implemented for the control of the simulations. The algorithms give ease of use also due to the fact that all important parameters can be altered and their effect examined from there.

All algorithms that were implemented along with the setup of the parameters used for the simulations are to be found in the Appendix, section Simulation Algorithms.

Chapter 5

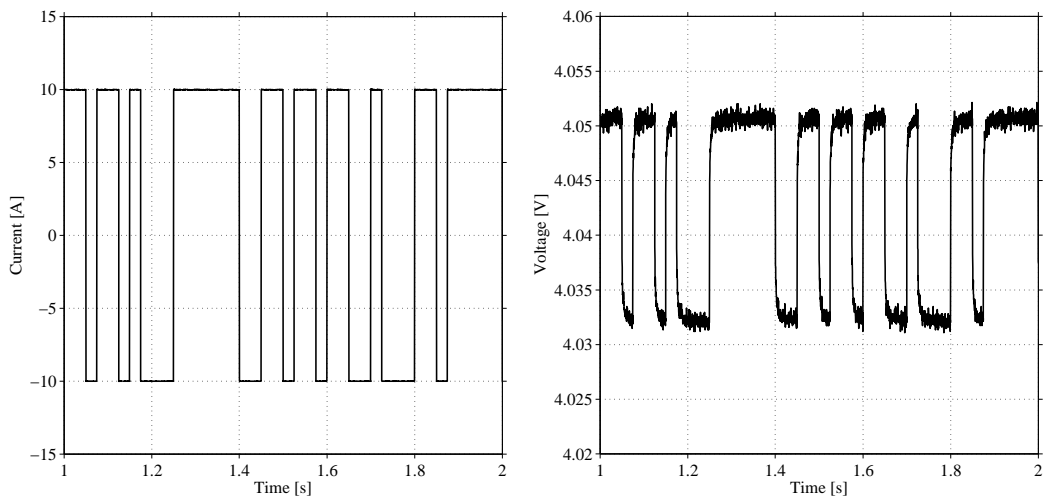
Experiments and simulations analysis

5.1 Experiment Results

Based on the set-up in Chapter 4.1, the experiment results are presented in this section. A nonparametric identification method is used to process the data. EIS measurements are performed at different SOC levels and temperatures to validate this method. The results show that the PRBS method is stable at different SOC levels and temperatures and it is possible to characterize the battery from its EIS.

5.1.1 Signal Processing

As discussed in the previous Chapters, an 8-bit PRBSs is selected to cover the desired frequency range. Here the PRBS with a 40 Hz clock frequency is presented to show the results. The input signal and corresponding output signal are shown in Fig 5.1. The input signal is a 10 A bipolar PRBS current with 40 Hz clock frequency. The voltage output is of a cell at 80% SOC level. Both the current and voltage data are logged by the GAMRY Reference 3000 and the sampling frequency is 4 kHz. As it can be seen, a 10 A current only cause about a 10 mV voltage change for this cell.

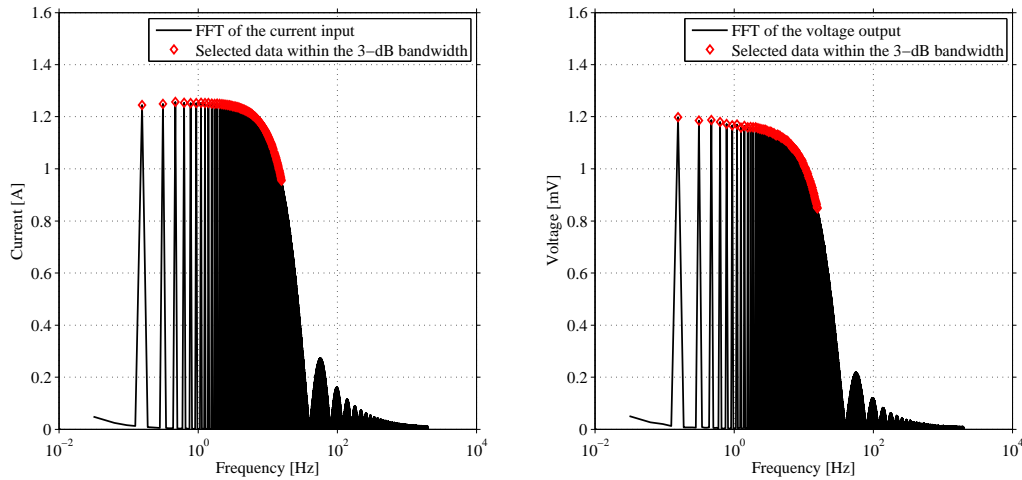


(a) 10 A Bipolar current input with 40 Hz switching frequency (b) Corresponding Voltage output logged by the GAMRY (80% SOC, 22 °C).

Fig. 5.1 Input and Output signal of the LG Chem 41 Ah battery by applying a PRBS signal.

To prepare the data for the following processing, the first step is to capture only the PRBS signal to make sure the data is periodic and with integer amount of cycles. The data during the rest time needs to be removed. After that, the *detrend* function in MATLAB can remove a linear trend of the data which will remove the DC offset. After that preparation, the data is analyzed in the frequency domain by using the Fast Fourier Transform (FFT).

Since the valid data for the impedance analysis is located within the 3-dB bandwidth at the specified frequency as described in Section 3.1, the data points need to be selected before calculating the impedance, as shown in Fig 5.2.



(a) FFT of the input current signal and selected current data within the 3-dB bandwidth. (b) FFT of the output voltage signal and selected voltage data within the 3-dB bandwidth.

Fig. 5.2 Data selection. The valid data is located within 3-dB bandwidth.

By inserting the selected data in the equations from (3.10) and (3.11), the impedance spectroscopy of the battery within the usable frequency range can be calculated. The final result of the calculated impedance at 80% SOC level in a Nyquist plot is shown in Fig 5.3, together with a reference EIS measurement.

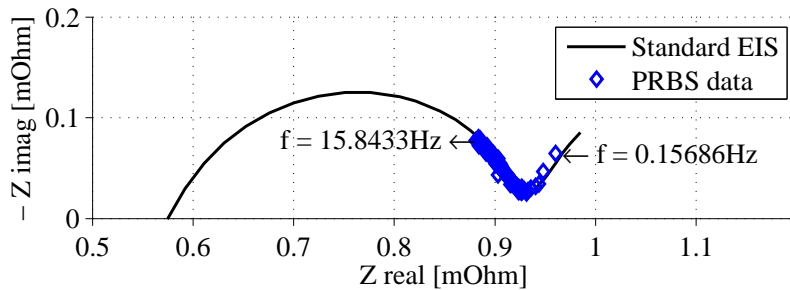


Fig. 5.3 EIS measurement in Nyquist plot with the PRBS method and the standard frequency sweep method at 80% SOC level 22 °C

The blue points are the PRBS measurement and the solid line is the EIS measurement from the GAMRY Reference 3000 which is a reference. It can be seen that the PRBS points are distributed along the reference EIS measurement, which can prove that the PRBS method is valid to produce an EIS measurement. The PRBS points covers the frequency range from 0.1568 Hz to 15.8433 Hz, which match the frequency range calculated in Table 3.1.

5.1.2 EIS Measurement at Different SOC Levels

PRBS measurements are performed at different SOC levels for the same cell to determine whether the PRBS method is stable and could be used for SOC indication. The test procedure is shown in Fig 4.2 and the results are shown in Fig 5.4. The cell is discharged and charged at 0.5 C by the GAMRY Reference 3000. The PRBS input is a 10 A bipolar current signal with 40 Hz clock frequency for all the SOC levels. The battery temperature is 22 °C controlled in the climate chamber.

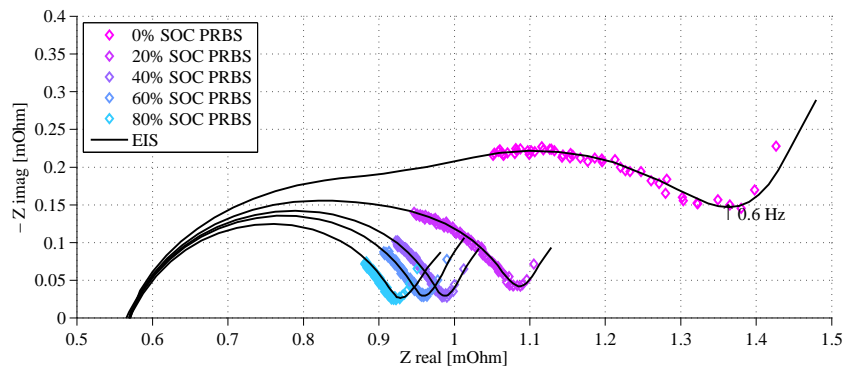


Fig. 5.4 EIS measurements with the PRBS method at 0%, 20%, 40%, 60% and 80% SOC levels at 22 °C.

The result shows that the PRBS method can be used to produce an EIS which is very similar as the standards method at each SOC level. It also shows that the impedance of the battery changes with the SOC level. The crossing of the X axis Z_{real} , which indicated the ohmic resistance R_{ohm} maintains the same value $0.57 \text{ m}\Omega$ at difference SOC levels while the charge transfer resistance R_{ct} increases as the SOC level decreases, similar trend in [3]. The values of the charge transfer resistance at difference SOC levels are listed in Table 5.1.

Table 5.1: The values of the charge transfer resistance at difference SOC levels showing that the impedance can be used to indicate the SOC level.

SOC level	Charge transfer resistance
0% SOC	$0.79 \text{ m}\Omega$
20% SOC	$0.52 \text{ m}\Omega$
40% SOC	$0.42 \text{ m}\Omega$
60% SOC	$0.39 \text{ m}\Omega$
80% SOC	$0.36 \text{ m}\Omega$

The values that are listed in Table 5.1 are also plotted in Fig. 5.5. As it can be noticed from both Fig. 5.4 and 5.5, the variation of the charge transfer resistance can be more easily detected at lower SOC levels.

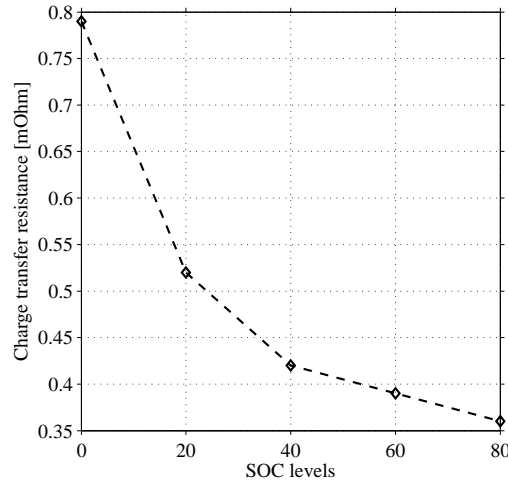


Fig. 5.5 The variation of the charge transfer resistance with the SOC level. It varies more significantly at lower SOC levels.

Apart from the value of the charge transfer resistance, the frequency where the R_{ct} is located is also interesting to be investigated. The information about the frequency comes from the standard EIS measurement since the PRBS measurement only covers a limited frequency range. A zoom of Fig. 5.4 is shown in Fig. 5.6 and the frequency related to the charge transfer resistance is marked at each SOC level. This frequency increases very slightly with the SOC level but it is always around 1 Hz. For the frequency related to the ohmic resistance, it is always around 600 Hz at different SOC levels.

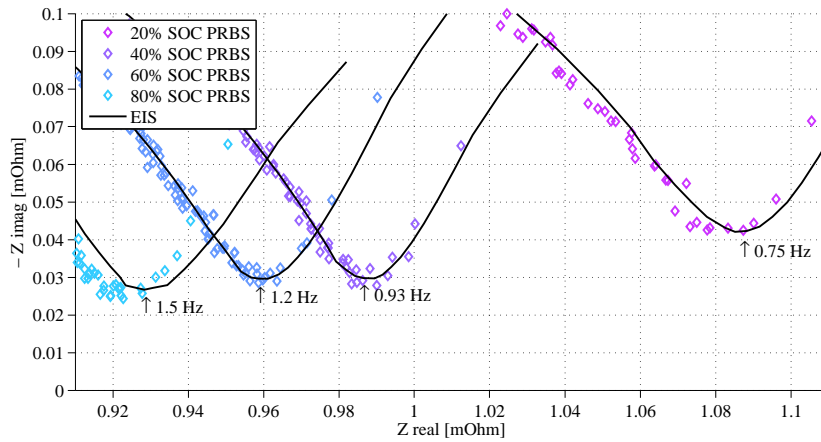


Fig. 5.6 A zoom in figure of the EIS measurements with the PRBS method at different SOC levels at 22 °C to indicate the frequency where the charge transfer resistance located.

5.1.3 EIS Measurement at Different Temperatures

The impedance of the battery is strongly dependent on the temperature. As most of the electric components, the impedance decreases as the temperature increase. The purpose of the experiments at different temperatures is to validate the PRBS method for variation of temperature and also to investigate the temperature effects on the battery impedance. The results are shown in Fig 5.7 and Fig 5.8, following the test procedure is shown in Fig 4.3. In the experiments, the PRBS input is a 10 A bipolar current signal with 40 Hz clock frequency for all temperatures. The SOC level is kept at 50% while the temperature is controlled by the climate chamber. As it can be seen, the temperature makes a significant impact on the battery impedance.

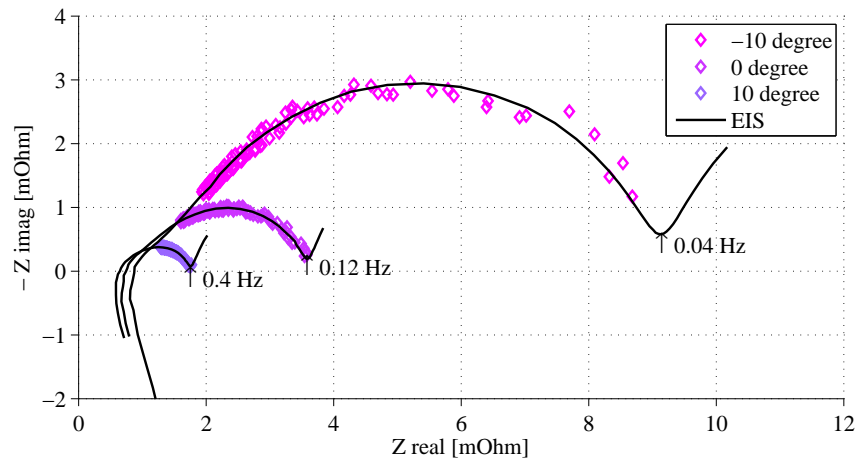


Fig. 5.7 The EIS measurement with the PRBS method at $-10\text{ }^{\circ}\text{C}$, $0\text{ }^{\circ}\text{C}$, $10\text{ }^{\circ}\text{C}$ at 50% SOC level for LG Chem 41 Ah cell. The PRBS points cover a frequency range from 0.15 Hz to 15 Hz.

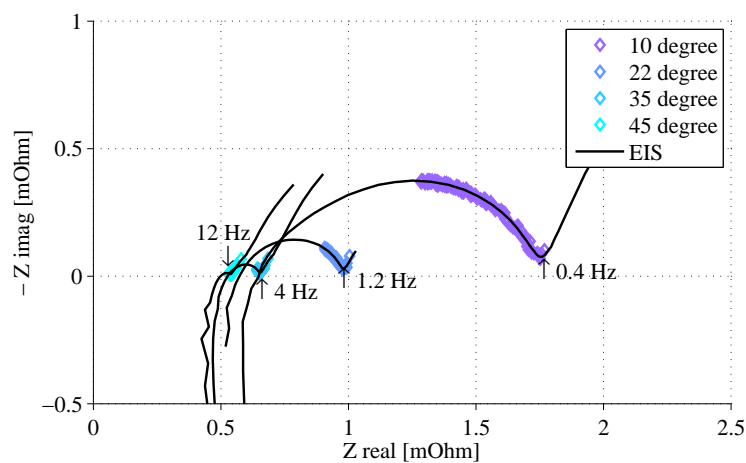


Fig. 5.8 The EIS measurement with the PRBS method at $10\text{ }^{\circ}\text{C}$, $22\text{ }^{\circ}\text{C}$, $35\text{ }^{\circ}\text{C}$, $45\text{ }^{\circ}\text{C}$ at 50% SOC level for LG Chem 41 Ah cell. The PRBS points cover a frequency range from 0.15 Hz to 15 Hz.

From the results it can be found that the frequency related to the charge transfer resistance or the ohmic resistance is affected more by the temperature than the SOC level. The values of the R_{ct} and R_{ohm} and their related frequency at different temperatures are listed Table 5.2. Since the frequency information comes from the standard measurement where the frequency sweep has a relatively large step at high frequency range, the frequency for the ohmic resistance is an approximate value.

Table 5.2: The values of the charge transfer resistance and ohmic resistance at difference temperatures with their related frequency.

Temperature	Frequency of R_{Ohm}	Value of R_{Ohm}	Frequency of R_{ct}	Value of R_{ct}
$-10\text{ }^{\circ}\text{C}$	900 Hz	$0.87\text{ m}\Omega$	0.04 Hz	$8.23\text{ m}\Omega$
$0\text{ }^{\circ}\text{C}$	700 Hz	$0.74\text{ m}\Omega$	0.12 Hz	$2.86\text{ m}\Omega$
$10\text{ }^{\circ}\text{C}$	600 Hz	$0.65\text{ m}\Omega$	0.4 Hz	$1.15\text{ m}\Omega$
$22\text{ }^{\circ}\text{C}$	500 Hz	$0.57\text{ m}\Omega$	1.2 Hz	$0.41\text{ m}\Omega$
$35\text{ }^{\circ}\text{C}$	300 Hz	$0.53\text{ m}\Omega$	4 Hz	$0.12\text{ m}\Omega$
$45\text{ }^{\circ}\text{C}$	180 Hz	$0.50\text{ m}\Omega$	12 Hz	$0.04\text{ m}\Omega$

The values listed in Table 5.2 are also plotted with the temperatures in Fig. 5.9. Both the charge transfer resistance R_{ct} and the ohmic resistance R_{ohm} decrease with the temperature increasing while the R_{ct} is more significantly reduced. At higher temperature, the frequency is higher for the R_{ct} and lower for the R_{ohm} .

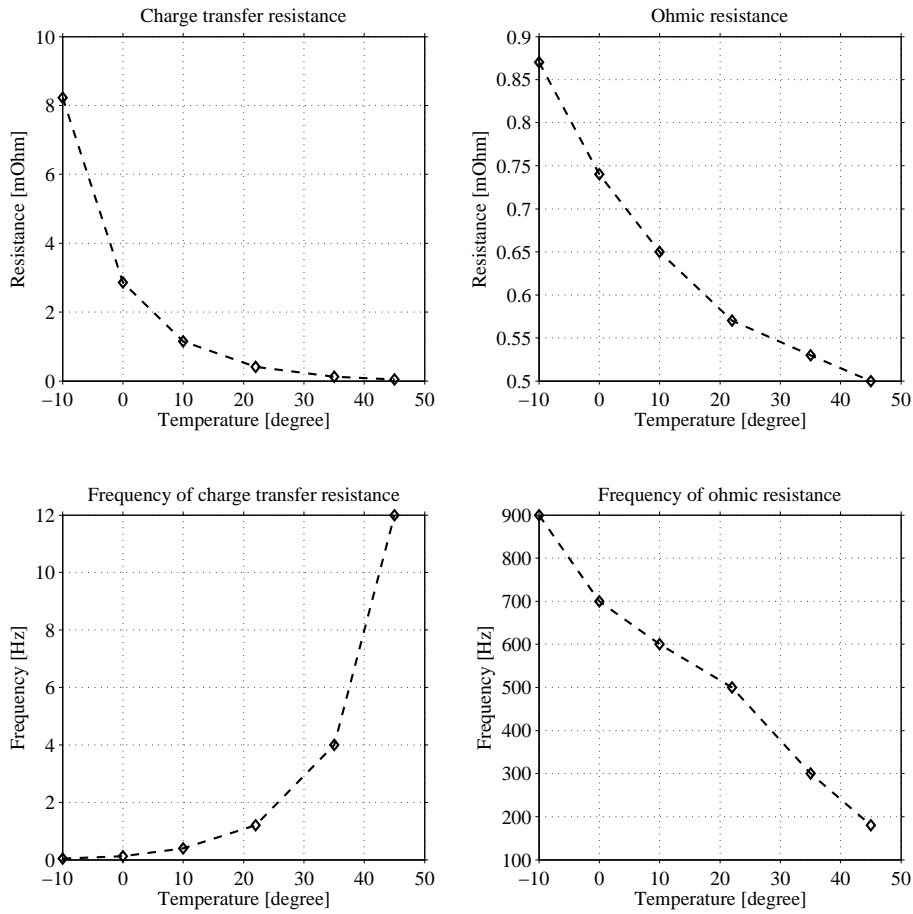


Fig. 5.9 The variation of the charge transfer resistance, the ohmic resistance and their related frequency with the temperatures.

5.1.4 Measurement Limitations

From Fig. 5.3 it can be seen that the PRBS method is valid to estimate an EIS characteristic in a frequency range between 0.15 Hz and 15.84 Hz with a 40 Hz clock frequency. In this frequency range, the information to indicate the SOC level can be extracted, as shown in Fig 5.4. However the information about the SOH is reflected from the ohmic resistance [2] and it has a extremely lower time constant. To capture the ohmic resistance, a faster PRBS with higher clock frequency is needed. The high frequency PRBS doesn't show a good result in the experiments. The problems and the limitations of the measurement will be discussed in this section.

During the measurement with a fast PRBS, a higher sampling frequency is used. In this case, voltage spikes can be observed, as shown in Fig. 5.10.

The reason is that there are inductive components existing in the connections with the cell, for example the connectors, and it is basically impossible to remove all the inductive connections.

For an inductor, the voltage is

$$u_L = L \frac{di}{dt} \tag{5.1}$$

So during the measurement, the current steps with high slew rate causes voltage spikes.

What is more, the cell is connected with the booster with a special designed cable from the GAMRY supplier which is used to reduce the skin effect. This cable cannot be changed or shortened and it contains a

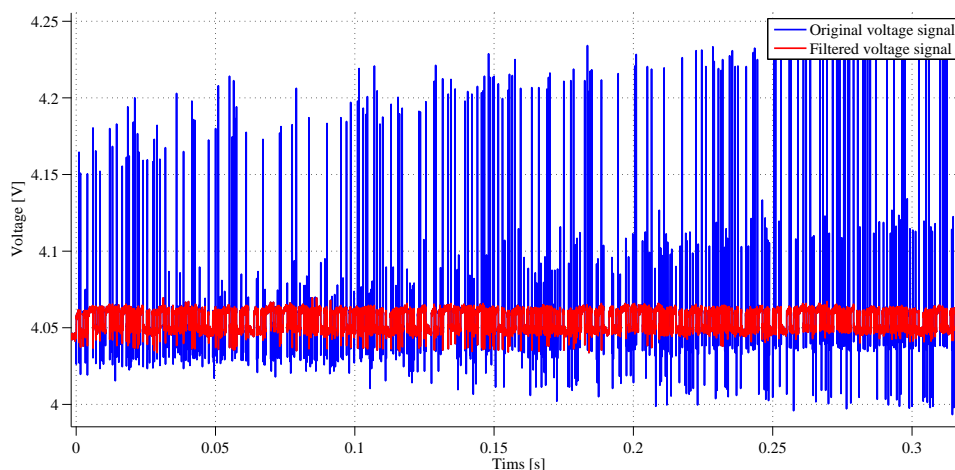


Fig. 5.10 Voltage spikes during the fast PRBS measurement with 50 kps.

large inductance, as shown in Fig. 5.11. Since in most of the applications the required signal for GAMRY is a sinusoidal wave, there is no problem by using this special designed cable. However, in this PRBS method it is very hard for the GAMRY to control the current steps properly with the inductance in the long cable. Therefore, there are overshoot in the current steps which makes the voltage spikes on the cell even worse.

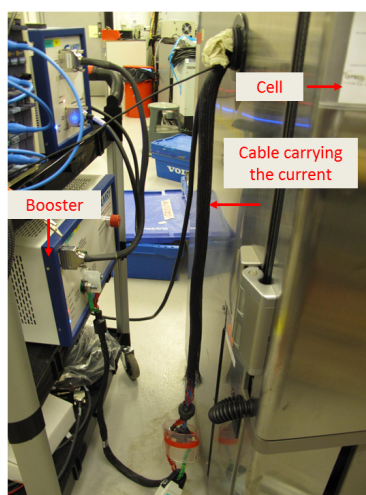


Fig. 5.11 The long cable between the booster and the cell which causes the switching spikes.

It is difficult to solve this problem by improving the hardware set-up since the cable cannot be replaced. One idea is to use a special designed software filter to remove the spikes. By using this software filter most of the spikes are removed as shown in Fig. 5.10.

However, this voltage signal presents the behaviors of both the cell and the inductive connections and the filter cannot distinguish these two behaviors. So the filter not only remove the spikes caused by the cable but also remove the useful information of the cell. A zoom of the original voltage signal and the filtered signal is presented in Fig. 5.12.

Actually, this problem is existing even in the previous measurements with a slow PRBS as well. The reason why it mainly affects the fast PRBS measurement is that the time constant of the inductive connections is in a similar range as the time constant of the ohmic resistance so both of their behaviors are mixed in the signal. When measuring the EIS with a slow PRBS focusing on the charge transfer resistance, a lower sampling frequency is used and the behavior of the inductive connection is hardly captured.

Finally, the impedance that is extracted from the filtered signal is shown in Fig. 5.13. The points at high frequency spread but they are still located in a expected range.

This result might be improved if a parametric identification method is applied. In this method, a cell

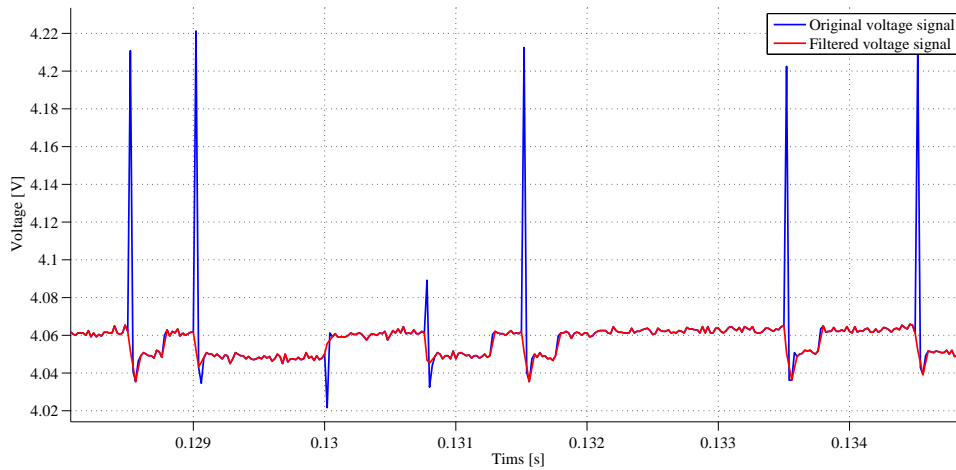


Fig. 5.12 A zoom of the original voltage signal and the filtered signal with 50 ksp.

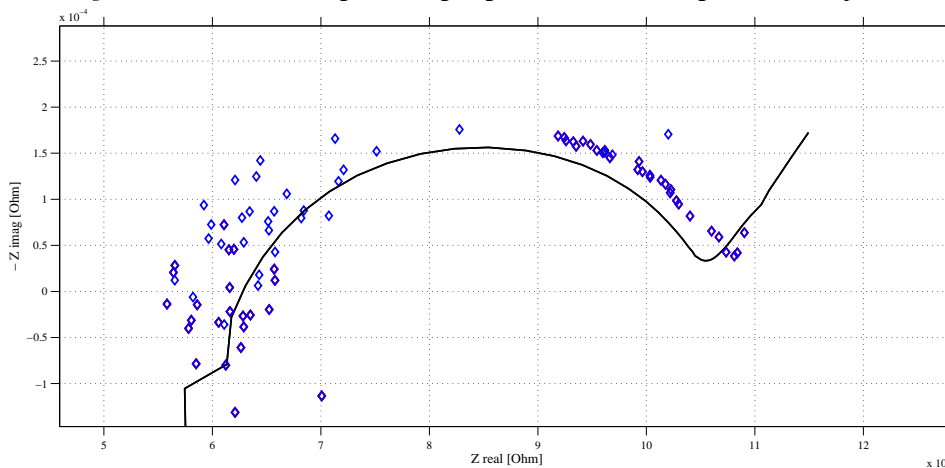


Fig. 5.13 EIS measurement in Nyquist plot with the PRBS method and the standard frequency sweep. The clock frequency of the PRBS is 4 kHz and the sampling frequency is 5 ksp.

model is required and then the voltage spikes caused by the inductive connections can be distinguished from the voltage response of the cell. However, the difficulty is that it is impossible to fit a simple linear model of the battery cell to describe its impedance accurately.

5.2 Simulation Results

The results of the simulation are respectively presented in the following subchapter. The results include the Nyquist behavior for the implementation of the EIS and PRBS methods and their comparison as a validation tool that the battery model can reproduce an EIS measurement response.

5.2.1 EIS Implementation

The EIS method has been implemented for a frequency range of 0.04 to 1000 Hz and is cooperating with the battery simulation model.

By having the phase difference, and from the impedance formula for the real and imaginary part, the Nyquist plot can be created, Fig. 5.14.

The Nyquist plot has been plotted for a vast range of frequency so it can be used as a reference tool of the PRBS method for any case needed to be examined and verified. The shape of the curve is presenting the EIS characteristics of a simple equivalent circuit.

Further result plots of the EIS implementation such as the Bode plot and the frequency-phase shift plot can be found in the Appendix.

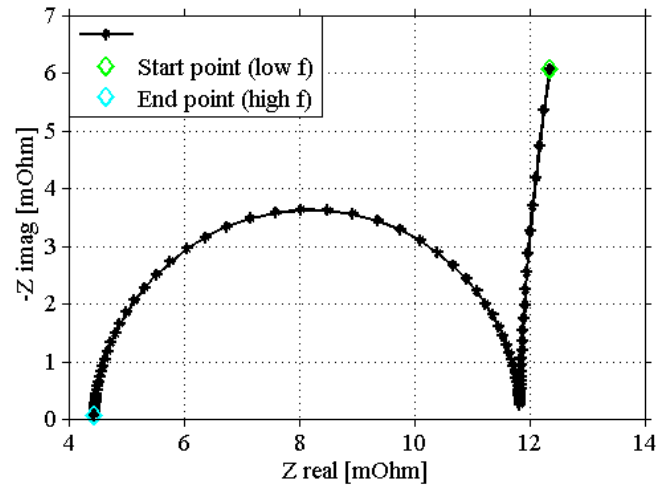


Fig. 5.14 Nyquist plot of the impedance for a frequency range of 0.04 to 1000 Hz

5.2.2 PRBS Implementation

The PRBS signal, applied in validation simulations is a square wave signal as described in section 2.4.2. It is created to be random and it can be seen in Fig. 5.15.

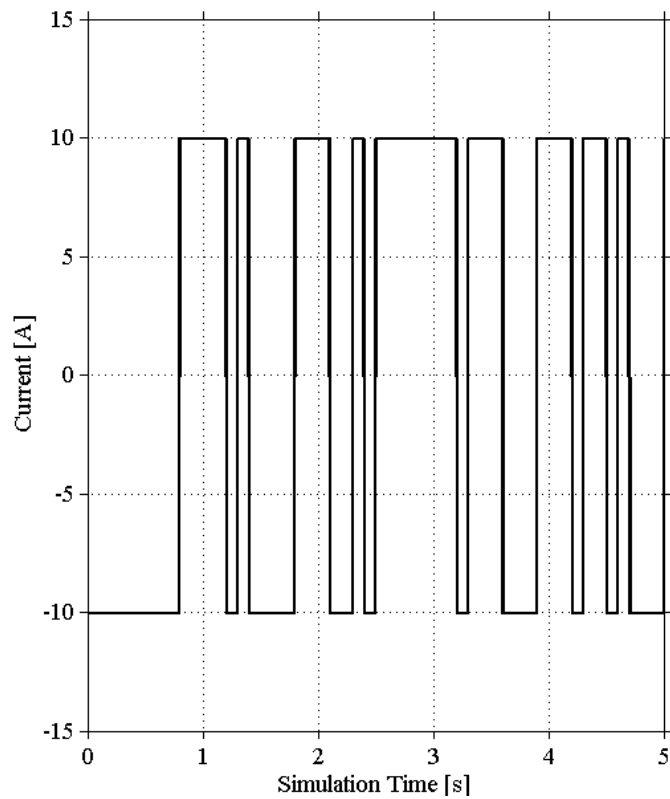


Fig. 5.15 Depiction of the PRBS signal used in the battery model

Afterwards, coupling the PRBS signal to the battery model, the voltage response achieved with the

PRBS current input can be seen in Fig. 5.16(a) and the Nyquist plot, Fig. 5.16(b).

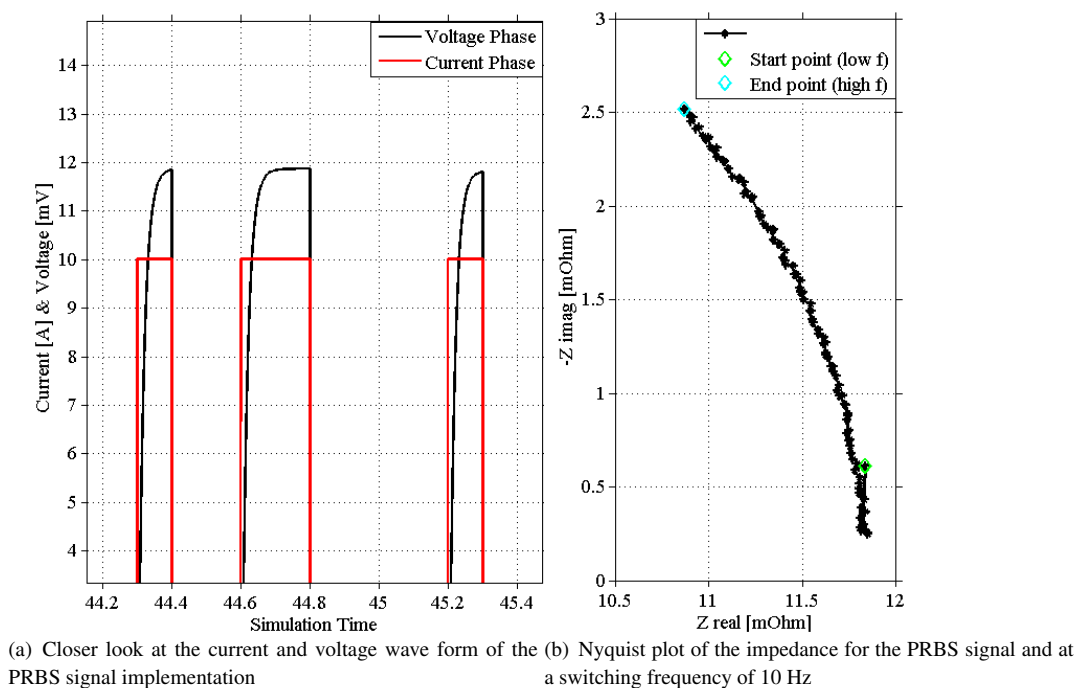


Fig. 5.16 PRBS implementation and creation of the Nyquist plot

5.2.3 Method Validation

For the PRBS implementation to be validated, the Nyquist plot of the EIS reference simulation is plotted against the output of the simulated PRBS. As it is seen in Fig. 5.17 the implementation shows no major deviations so it is assumed to be operating accurately.

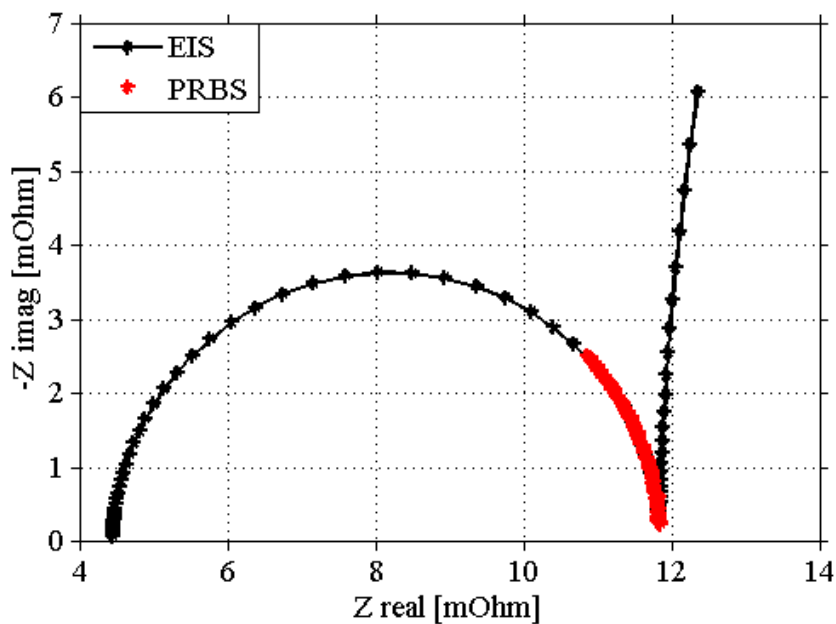
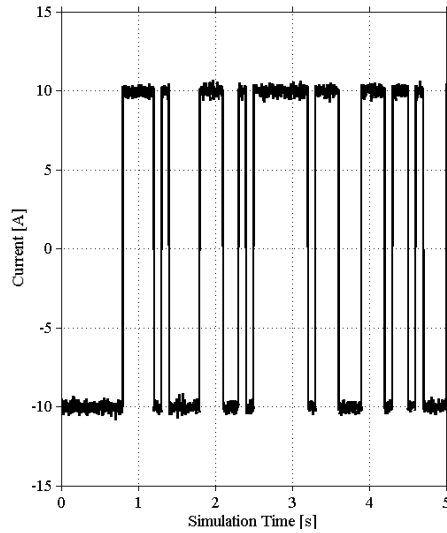


Fig. 5.17 Comparison of the EIS and PRBS at the low frequency area

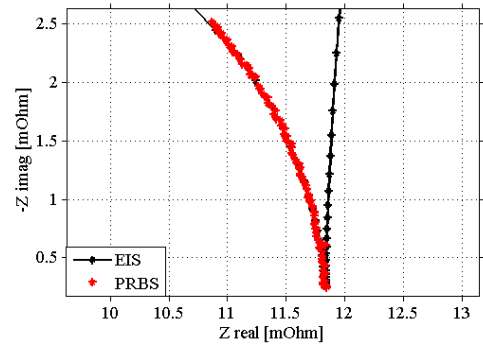
What has to be added though in the PRBS signal in order to represent real life conditions more accu-

rately is noise. The different type of noise to be implemented and examined is white noise at low and high frequencies.

For the white noise implementation, a percentage of the current amplitude shall be added as noise power and the effect of each change is examined.

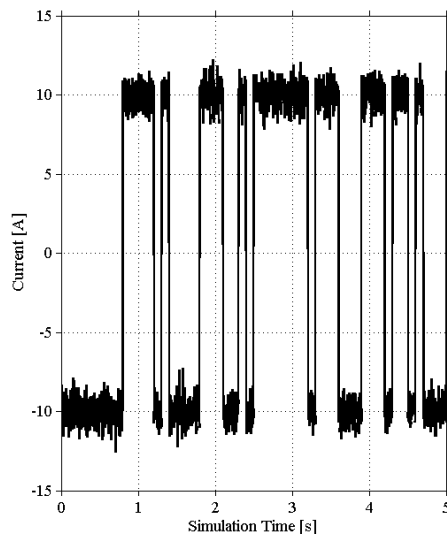


(a) PRBS signal with 1% white noise.

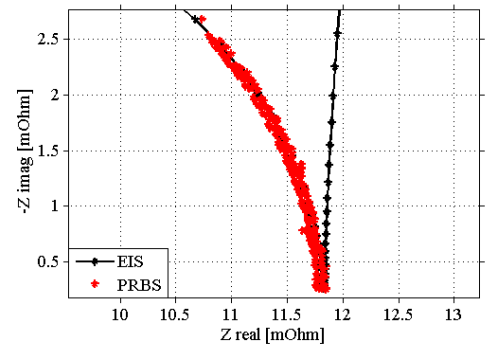


(b) Comparison of the EIS and PRBS for white noise 1%t.

Fig. 5.18 PRBS signal effect and comparison for a white noise addition of 1%.



(a) PRBS signal with 10% white noise.



(b) Comparison of the EIS and PRBS for white noise 10%t.

Fig. 5.19 PRBS signal effect and comparison for a white noise addition of 10%.

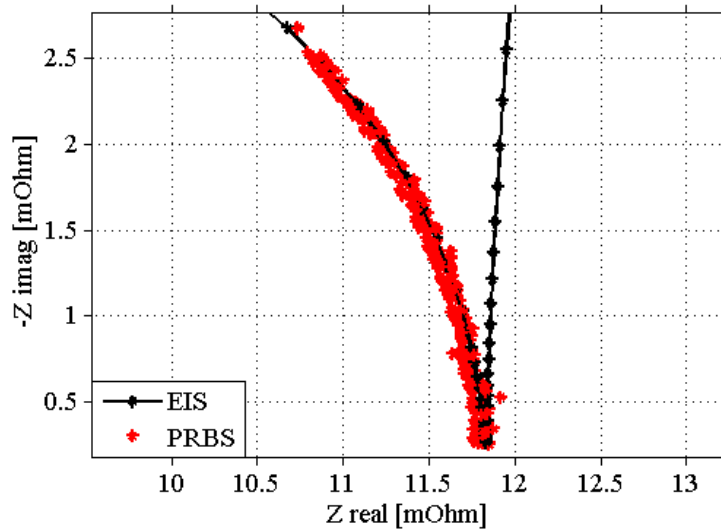


Fig. 5.20 Comparison of the EIS and PRBS for a white noise addition of 25%

From figures 5.18(a) and 5.19(a) the effect of the white noise on the PRBS signal can be observed. Subsequently, Fig. 5.18(b) and 5.19(b) depict the behaviour of the PRBS signal in comparison to EIS reference. Above a noise to signal ratio of 25% it can be observed from Fig. 5.20 that the deviation in the results is becoming higher.

With the same principle in mind, the white noise will be implemented for the high frequency area of the PRBS signal, that have not yet been tested experimentally in the laboratory environment due to equipment limitations.

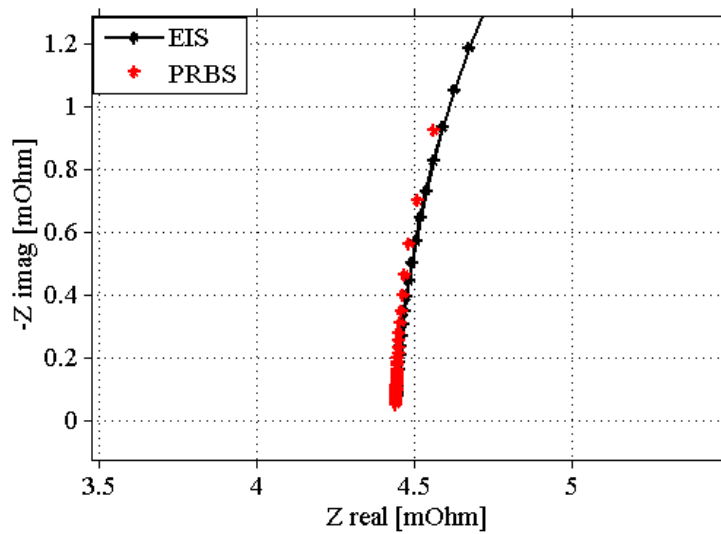


Fig. 5.21 Comparison of the EIS and PRBS at the high frequency range, no noise implemented

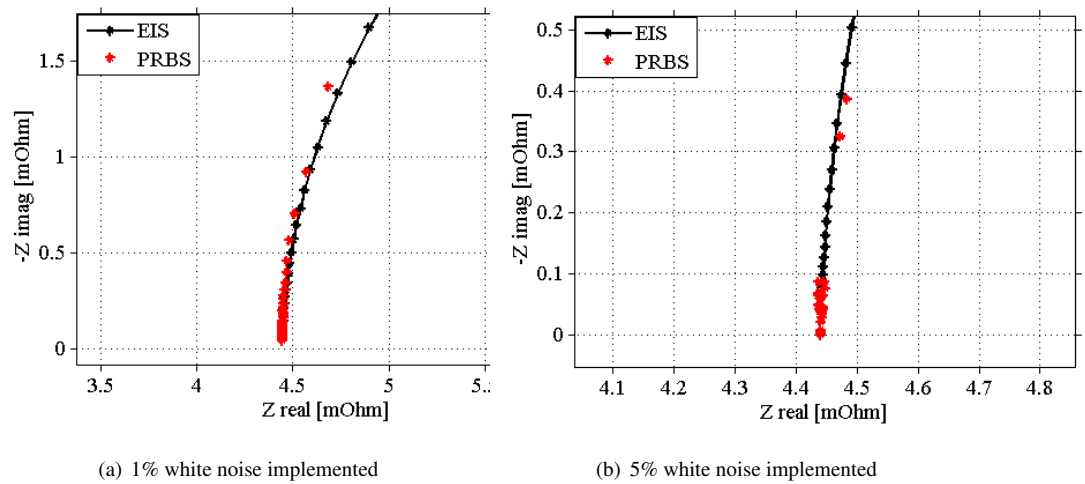


Fig. 5.22 Comparison of the EIS and PRBS at the high frequency range

It can be seen in Fig 5.21 that for no noise implemented in the PRBS, the signal follows the curvature of the reference almost in a similar manner. The small deviation existing can be due to minor differences in the method implementation. For a noise to signal ratio addition of 1% and 5%, depicted in figures 5.22(a) and 5.22(b) accordingly, the noise implementation of 1% shows an insignificant deviation and remains within the lines of the reference, whereas the 5% presents significant differences on its response. As an outcome, what can be said that both for low and high frequency PRBS, the sensitivity response to noise addition is considered to be the same, especially in the low noise area recommended for further use.

Taking into consideration the results mentioned above and the behaviour of the PRBS in comparison to the EIS, shown in Fig. 5.23, a white noise with a signal to noise ratio of 1% will be used for further experiments to be simulated for the validation of the PRBS method. A 1% implementation of noise represents a respectable amount of noise in the battery model implementation but at the same time does not create major deviations in the results.

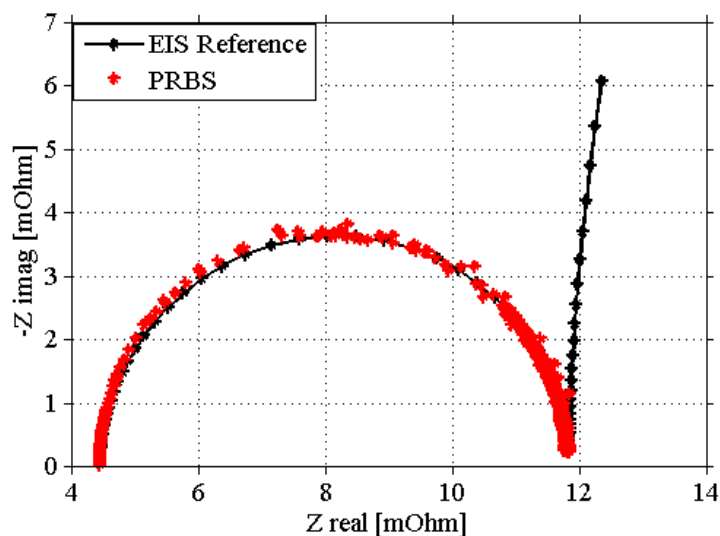


Fig. 5.23 EIS and PRBS methods in the whole frequency range, white noise addition of 1%

For the complete validation of the PRBS method, various parameters such as the SOC, SOH and more will be examined for different values and their effect in comparison to the reference will be observed. All parameters to be altered for the simulations to be run can be found in detail in the Appendix, Fig. B.1.

The SOC influence can be observed in Fig. 5.24 and Table 5.3. Even though the values of the charge transfer resistance do not get such a large impact, nonetheless the influence of the SOC is visible on it. The closer the values of the SOC to the reference the closer the charge transfer resistance is as well.

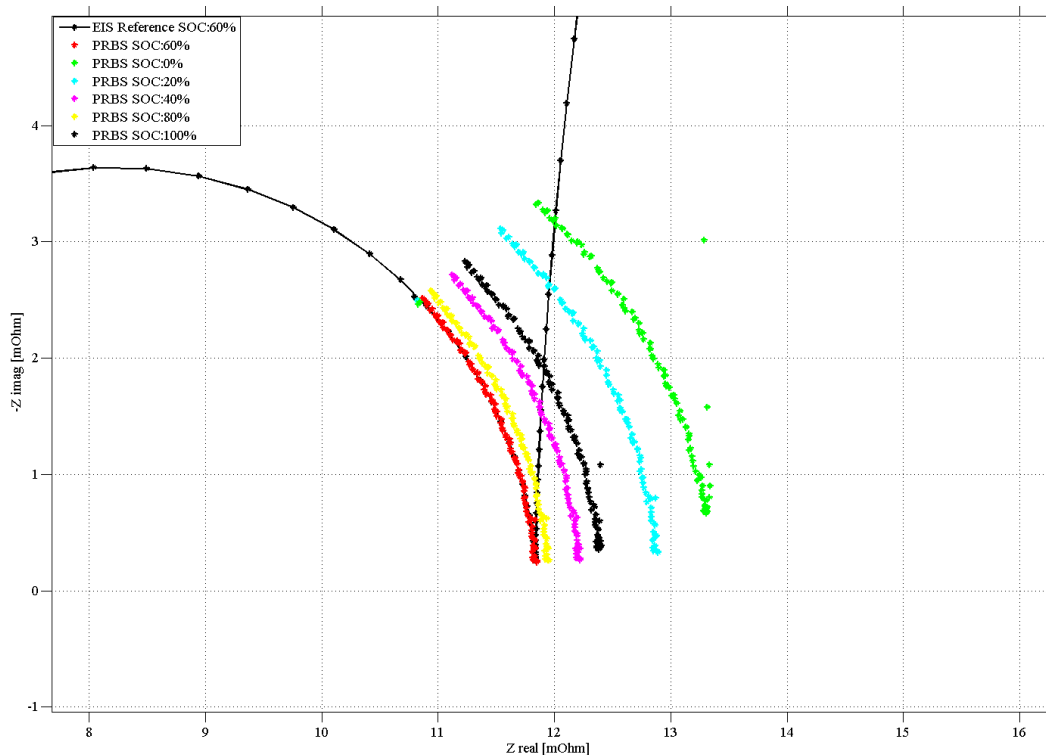


Fig. 5.24 SOC influence in the PRBS method against the EIS reference in the Nyquist plot

Table 5.3: Charge transfer resistance influence from SOC

SOC level	Charge transfer resistance
0% SOC	8.8 $m\Omega$
20% SOC	8.4 $m\Omega$
40% SOC	7.8 $m\Omega$
60% SOC	7.4 $m\Omega$
80% SOC	7.6 $m\Omega$
100% SOC	8.05 $m\Omega$

The temperature can be said to be a very important factor when it comes to battery impedance and this can be observed in the effect it has on the Nyquist plot, depicted in Fig. 5.25.

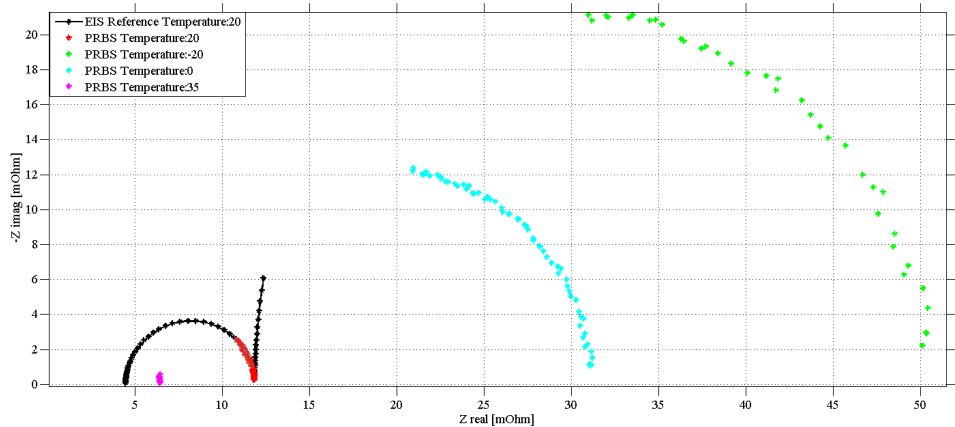


Fig. 5.25 Temperature influence in the PRBS method against the EIS reference in the Nyquist plot

The switch frequency of the PRBS signal has been examined in order to see if by changing its value, there are differences in the results. As depicted in Fig. 5.26, even with large changes in the switch frequency value, the Nyquist plot remains close to the reference.

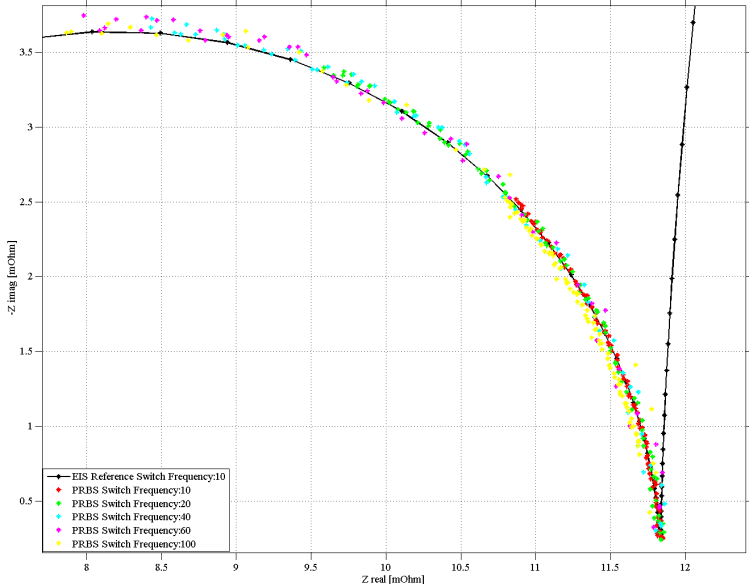


Fig. 5.26 Switch frequency influence in the PRBS method against the EIS reference in the Nyquist plot

The cycle time of the PRBS signal, even though it increases the computational time significantly, nonetheless it affects the accuracy of the results. As seen in Fig. 5.27, the higher the cycle time value the closer the PRBS is coming to the EIS and the lower the value the more deviations can be observed.

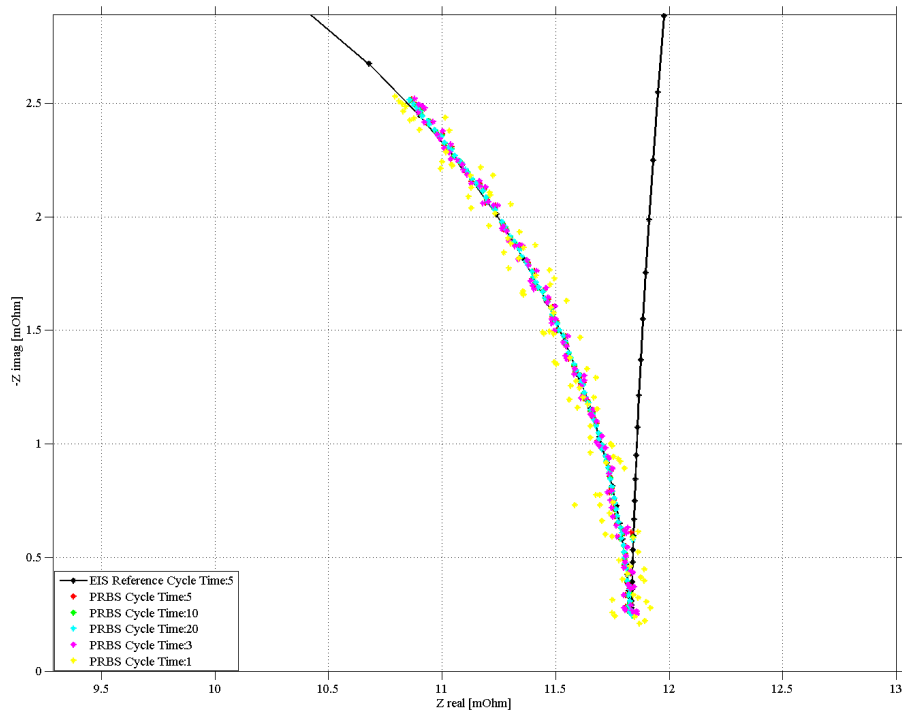


Fig. 5.27 Cycle time influence in the PRBS method against the EIS reference in the Nyquist plot

Minor deviations in the results along with random points being presented at extraordinary positions can be justified by implementation differences and noise interactions that affect the results. The quality of the results nonetheless is considered high, meaning that the validation of the PRBS method implementation has been completed with the means of the EIS method as a reference.

Further figures depicting the influence of all the above parameters in their lowest or highest values used, in addition to their comparison and correlation to the reference method can be found in the Appendix, section EIS, PRBS and validation figures.

Chapter 6

PRBS Implementation in the Vehicle

An excitation current like PRBS need to be generated and applied on the battery to perform an EIS measurement in a hybrid electric vehicle or an electric vehicle. Instead of using an additional equipment, the drive line existing in the vehicle can be used to perform an on-board test. The electric motor can act as the load to generate an excitation current since it is more controllable and has a faster response compared to other loads. A simulation is made to examine to possibility of obtaining an excitation current by controlling the electric motor.

6.1 Motor Model and Control Algorithm

The electric motor used in the simulation is a permanent magnet synchronous motor (PMSM) and the field oriented control (FOC) with field weakening is used to control the motor. The dynamic model of a PMSM and the FOC are described here.

6.1.1 Motor Model

The PMSM consists a rotor built with permanent magnets to provide the magnetic filed. The windings are distributed in the stator and fed with three-phase voltage. The voltage and current in the stator can be presented in $\alpha\beta$ -coordinates in order to simplify the analysis. An amplitude invariant transformation is

$$\begin{bmatrix} U_\alpha \\ U_\beta \end{bmatrix} = \begin{bmatrix} \frac{2}{3} & -\frac{1}{3} & -\frac{1}{3} \\ 0 & \frac{1}{\sqrt{3}} & -\frac{1}{\sqrt{3}} \end{bmatrix} \begin{bmatrix} U_a \\ U_b \\ U_c \end{bmatrix} \quad (6.1)$$

The transformation is a mathematical method to convert the three-phase signal to two-phase.

In field oriented control, $\alpha\beta$ quantities are transfered into dq-coordinates. The dq-coordinates rotates at the speed of the magnetic field and the d-axis is aligned with the rotor flux.

$$\begin{bmatrix} U_d \\ U_q \end{bmatrix} = \begin{bmatrix} \cos(\theta) & \sin(\theta) \\ -\sin(\theta) & \cos(\theta) \end{bmatrix} \begin{bmatrix} U_\alpha \\ U_\beta \end{bmatrix} \quad (6.2)$$

where θ is the angle between d-axis and α -axis.

In the dq-coordinates, the electric model can be described with

$$\begin{cases} u_{sd} = R_s i_{sd} + L_s \frac{di_{sd}}{dt} - \omega_r L_s i_{sq} \\ u_{sq} = R_s i_{sq} + L_s \frac{di_{sq}}{dt} + \omega_r L_s i_{sd} + \omega_r \Psi_m \\ T_e = \frac{3n_p}{2} \psi_m i_{sq} \end{cases} \quad (6.3)$$

where ω_r is the speed of the flux linkage [36].

The mechanical model is presented by

$$\frac{J}{n_p} \frac{d\omega_r}{dt} = T_e - T_L - b\omega_r \quad (6.4)$$

where T_e is the electric torque produced by the motor and T_L is the load torque. $b\omega_r$ presents the mechanical damping.

The meaning and value for the other parameters are shown in Table 6.1. The value of the parameters are from the simulation model of the Volvo Prototype Machine (VPM). The parameter J and b is for a stand alone PMSM, i.e. not mounted in the vehicle.

Table 6.1: Motor parameters used in the simulation from Volvo Prototype Machine (VPM).

	Parameter	Value
Stator resistance	R_s	0.0273Ω
Inductance	L_s	$0.738 mH$
Inertia	J	$0.0419 kgm^2$
Number of pole-pairs	n_p	8
Viscous damping	b	$0.01 Nm.s/rad$
Flux linkage	Ψ_m	$0.1283 Wb$

6.1.2 Motor Controller

In a HEV/EV an electric motor is typically involved in the propulsion. The electric motor is commanded to generate a required torque which is calculated with the position of the gas pedal. The electric torque produced by the motor is related to the stator current, as shown in (6.3). Accordingly, a very important part of the motor controller is the current controller which is shown in Fig. 6.1.

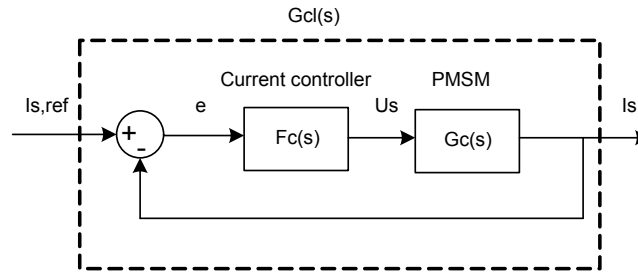


Fig. 6.1 A block diagram of the basic close loop motor controller.

The idea of the controller is to make the close loop system $G_{cl}(s)$ to be a first-order low-pass filter [37]. So the current controller $F_c(s)$ has the same bandwidth as $G_c(s)$ which represents the PMSM. This forms a proportional-integral (PI) controller

$$F_c(s) = k_{pc} + \frac{k_{ic}}{s} \quad (6.5)$$

where the two parameters k_{pc} and k_{ic} are the proportional gain and the integral gain. They can be calculated based on the motor parameter and the bandwidth of the controller.

$$k_{pc} = \alpha_c L_s, \quad k_{ic} = \alpha_c^2 L_s \quad (6.6)$$

The controller bandwidth α_c is chosen to be 732 rad/s which is designed by Volvo.

As the motor speed increase, the stator voltage reaches its maximum value, which is limited by the output voltage of the battery. If a higher speed is required, a field weakening controller needs to be implemented. The field weakening is obtained by ordering a negative d-axis current reference. More details about the field weakening are discussed in [37].

In many HEVs/EVs, the electric motors are not only used for the propulsion, but also as generators to collect the energy during the regenerative braking. The electric motor operates as a generator, converting the mechanical energy into electric energy. It helps the vehicle to brake and on the other hand the current is fed back to the battery which charges the battery. To achieve a regenerative braking, the motor is given a negative torque reference, which is equivalent to a negative current reference.

6.2 Simulation of the Excitation Signal on the Drive Line

The simulation model is based on an assignment from the course ENM075 Electric drives 2 at Chalmers. The simulation is performed in MATLAB. It consists of a battery model, a three-phase inverter, an electric motor, a motor controller and a modulator, as shown in Fig. 6.2.

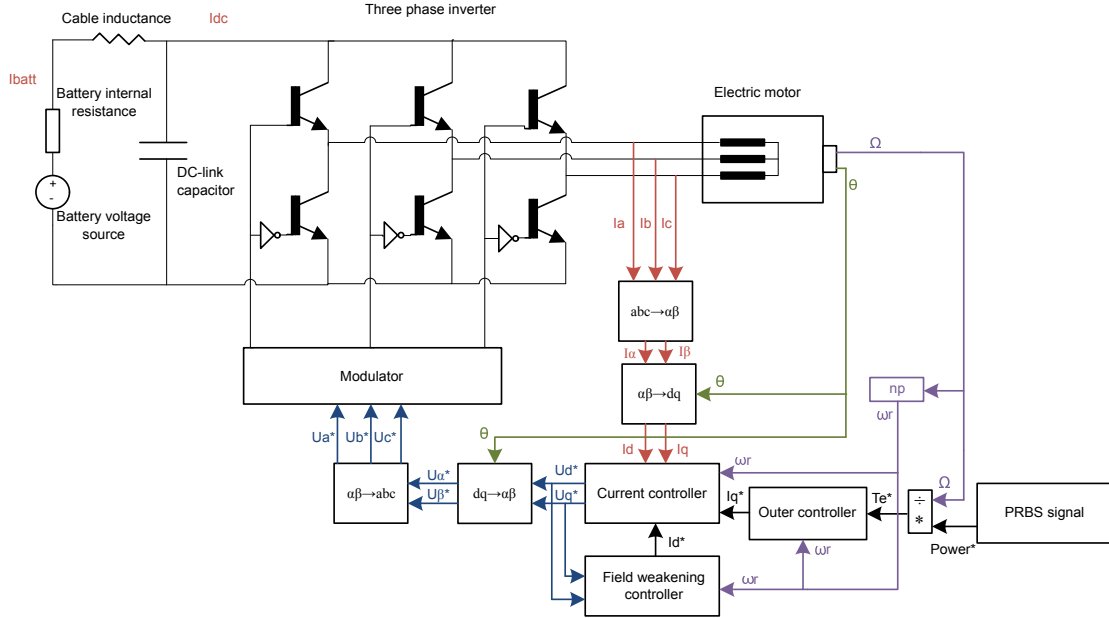


Fig. 6.2 A simplified schematic of the drive line in an electric vehicle.

6.2.1 Simulation Model of the Drive Line

The battery model used in this simulation is a constant voltage source with an internal resistor. The reason is that during the short simulation time, it can be assumed that the battery SOC does not change and accordingly the open circuit voltage is constant. For the whole drive line simulation, the voltage deviation on the battery pack can be simplified to be the voltage drop over a resistance. Compared to a simplified battery model, an accurate battery model will not affect the motor behavior much but it will increase the computation load. This is why in this simulation a simplified battery model is used.

The inverter contains six switches which are assumed to be ideal. The switching behaviors, including the turn-on time and turn-off time, are ignored. The DC-link capacitor is taken into consideration since it will eliminate the high frequency component in the battery current. The inductance in the cable connecting the inverter and the battery will have a similar effect on the battery current as the DC-link capacitor. However it slows down the simulation speed a lot so it is not verified in this thesis due to the time limitation.

The motor model is implemented by Volvo in dq-coordinates with the parameter values mentioned above.

As discussed before, the motor controller is using FOC with field weakening. A discrete simulation is used and the sampling time is 8 kHz, the same as the switching frequency in the inverter. In most of the vehicles, there is a slew rate limitation of the torque so that the torque of the vehicle will not change too rapidly. Since the detailed data is not available during the thesis, it is assumed that there is no limitation on the torque step in the simulation.

The target of the simulation is to apply an excitation current like PRBS on the battery pack. If the battery pack voltage is assumed to be constant, there will be a power PRBS applied to the battery.

$$P(t) = UI(t) = T_e(t)\omega(t) \quad (6.7)$$

Therefore, the torque reference that is to be sent to the controller is

$$T_{ref} = \frac{PRBS \text{ power signal}}{\omega} \quad (6.8)$$

Finally, a pulse-width modulation (PWM) is used in the modulator to control the switches in the inverter. The important parameter values in the simulation are list in Table 6.2.

Table 6.2: Drive line parameters and control parameters used in the simulation.

	Parameter	Value
Battery voltage source	V_{batt}	600 V
Battery internal resistance	R_{batt}	0.1 Ω
Cable inductance	L_{cable}	N/A
DC-link capacitor	C_{dc}	5*100 μF
Bandwidth of the controller	α_c	732 rad/s
Sampling frequency/Switch frequency	f_s	8 kHz

6.2.2 Speed Operation Range

During the EIS measurement, the vehicle is assumed to be in the garage and in neutral position. The electric motor is only attached with the clutch which adds about 50% of the inertia. The inertia is very small and the speed of the motor can be easily changed under a small torque. So the power amplitude of the excitation signal cannot be too large otherwise the motor will accelerate over the operation range.

On the other hand, the PRBS power signal needs to be as large as possible to achieve a high current in and out of the battery, since a good signal to noise ratio (SNR) needs to be reached in both current and voltage signals with the small impedance of the battery.

The torque/speed and power/speed curves of the motor are shown in Fig. 6.3. The idea is to keep the motor operation under a maximum possible torque and speed range to reach the maximum possible power. During the operation range, field weakening may occur depending on whether the voltage limitation is reached.

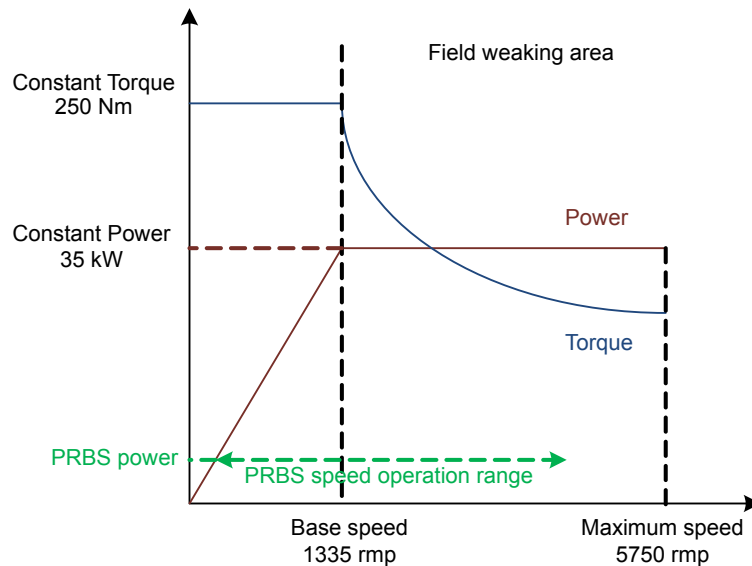


Fig. 6.3 The Torque/Speed and Power/Speed curves of the PMSM.

6.2.3 Parameters Selection of the PRBS in the Drive Line Simulation

Desired frequency range

The first step to decide the parameters is to decide the lowest frequency that the excitation signal will contain. Assume the testing object has the same chemistry as the battery cell used in previous experiments. So the interesting frequency point is around 1 Hz. To capture the charge transfer resistance R_{ct} , the desired

lowest frequency is selected to be 0.2 Hz. The frequency resolution is the same as the lowest frequency point, 0.2 Hz, shown in (3.5).

The second step is to select the desired highest frequency while the highest usable frequency in the PRBS is only dependent on the clock frequency, shown in (3.4). There are several factors that limit the slew rate of the current step in the drive line simulation, including the bandwidth of the current controller and the DC-link capacitor. Other factors, for example the torque step limitation and the cable inductance, will have similar effects but they are not included in this simulation. The reasons are explained in the previous section. Due to these limitations, the clock frequency of the PRBS is preferred to be as low as possible so that the slow slew rate can be neglected. On the other hand, the clock frequency needs to be high enough to offer a wide enough frequency range for the cell in question. Here the clock frequency is selected to be 12.5 Hz.

Suitable PRBS bit and cycle number

After the lowest frequency point and the clock frequency are defined, the PRBS bit length can be calculated according to (3.3). A 6-bit PRBS is decided to use in the drive line simulation.

Three cycles of the PRBS is simulated due to the computation load. More cycles can improve the result but it is not a key factor in this simulation.

PRBS offset and initial state

In the laboratory experiments, a bipolar PRBS is used to avoid an open circuit voltage and SOC level deviation. However, in the drive line simulation, the motor is not running in an ideal environment. With a bipolar PRBS, no power flows from the battery to the motor and the motor speed will decrease due to the mechanical damping and friction losses. Therefore, a certain offset in the bipolar PRBS is needed to keep the motor running at a certain speed range.

Another factor that needs to be chosen is the PRBS initial state. In the thesis the PRBS is generated by the linear shift registers and there is an initial value in each register. By default, all the initial values are set to be 1. In this case, the motor will keep accelerating in the first several clock periods and this is the longest acceleration time during the PRBS test, which limits the initial speed of the motor and the power amplitude. This long acceleration time can be interrupted by starting the PRBS at one of the middle states.

After all, since the power amplitude, the PRBS offset and the initial PRBS state are coupled to each other, it is very hard to decide their values through calculation. An arbitrary way to decide these parameters is by tuning the parameters to get a set of values. To save the simulation time, a simplified simulation is used as shown in Fig. 6.4. The electric behavior of the motor is neglected since its time constant is much faster than the mechanical time constant. Only (6.4) is implemented in the motor model, so that a large amount of the computation load is reduced.

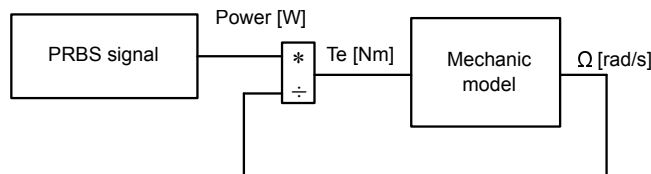


Fig. 6.4 A simplified mechanical motor model to defined the speed operation range and power amplitude for the PRBS test.

Two sets of parameters will be used in the simulation according to tuning results in the simplified model, shown in Table 6.3 and 6.4. The set-up 1 comes from by aiming to have the maximum power amplitude while the set-up 2 is based on avoiding the field weakening. The reason and its analysis will be explained in the results chapter.

Table 6.3: Set-up 1 PRBS parameters used in the drive line simulation with low power amplitude

Parameter	Value
PRBS clock frequency	12.5 Hz
PRBS bit length	6-bit
PRBS power amplitude	2500 W
PRBS offset	15%
PRBS initial state	011000
Motor initial speed	2000 rpm

Table 6.4: Set-up 2 PRBS parameters used in the drive line simulation with high power amplitude.

Parameter	Value
PRBS clock frequency	12.5 Hz
PRBS bit length	6-bit
PRBS power amplitude	4000 W
PRBS offset	14.5%
PRBS initial state	011000
Motor initial speed	3000 rpm

6.3 Results and analysis

The results from the simulations of the excitation signal on the drive line are presented here. Both of the set-ups in Table. 6.3 and 6.4 are examined.

Results of the set-up with low power amplitude

With the low power amplitude 2.5 kW, the motor is running in a speed range between 600 revolutions per minute (RPM) and 3000 rpm with an initial speed of 2000 rpm. During the simulation, the excitation signal repeats for three cycles and the power offset makes it possible for the motor to operate in this speed range.

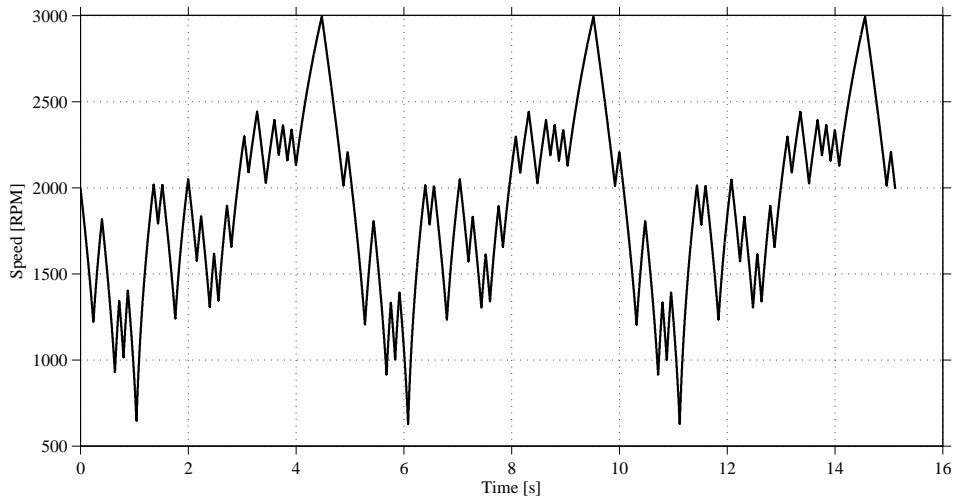


Fig. 6.5 Operation speed range during the simulation with 2.5 kW power amplitude.

The current on the DC side of the inverter and the current on the battery pack are shown in Fig. 6.6. The DC-link capacitor limits the rise time of the current steps and eliminates the very high frequency components.

As discussed before, a good PRBS signal requires sharp current steps but unfortunately there are a lot of factors that limit the rise time of the current steps in the drive line. In Fig. 6.7, a current step is presented and the rise time is about 2 ms. This value will be even longer if the cable inductance and especially the torque limitation are taken into consideration.

The excitation current signal in frequency domain is shown in Fig. 6.8. It looks very similar to the PRBS signal in frequency domain in Fig. 3.3(b) and it contains a signal in the desired frequency range

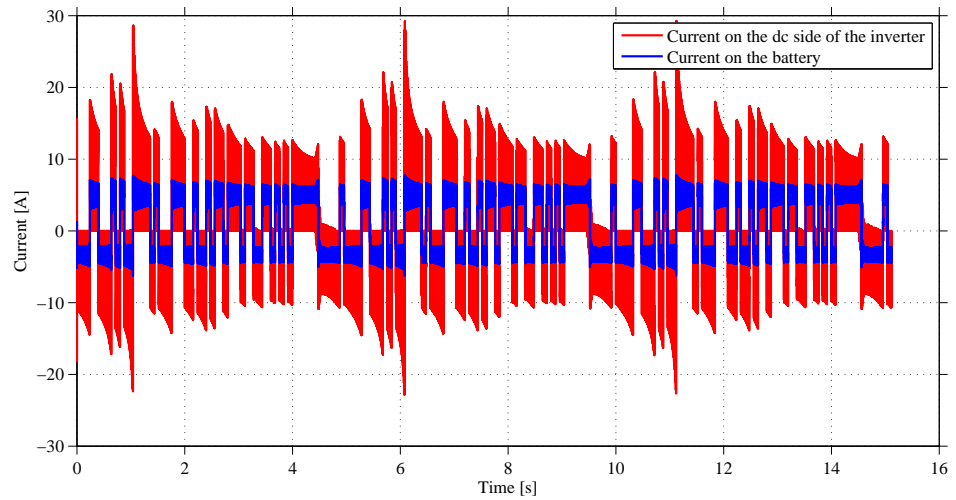


Fig. 6.6 The DC-link current and battery pack current during the simulation with 2.5 kW power amplitude.

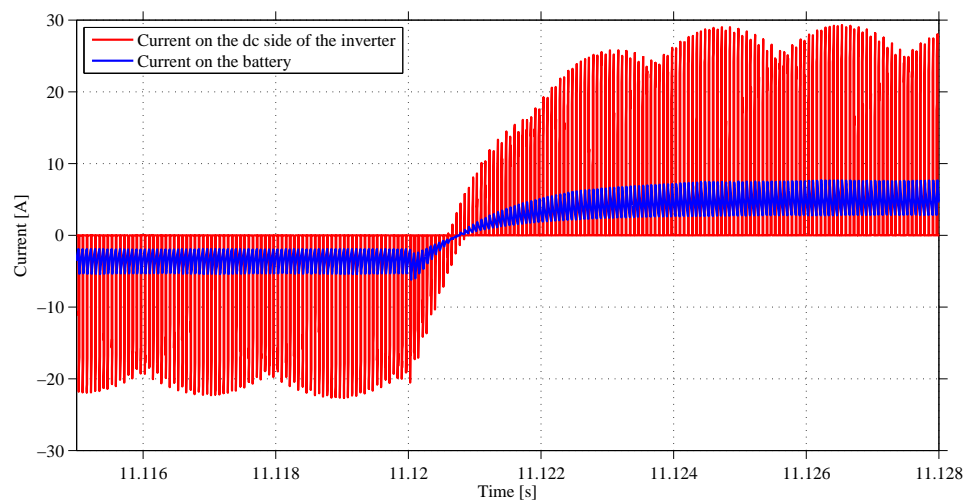


Fig. 6.7 A zoom of the DC-link current and battery pack current during the simulation showing the rise up time.

which is between 0.2 Hz and 5 Hz. The maximum current amplitude is around 1 A. For a battery pack whose impedance is several hundreds of $m\Omega$, this 1 A current will only cause a voltage change less than 1 V, which is very hard to measure on a 600 V battery pack. Therefore, a high current amplitude is needed.

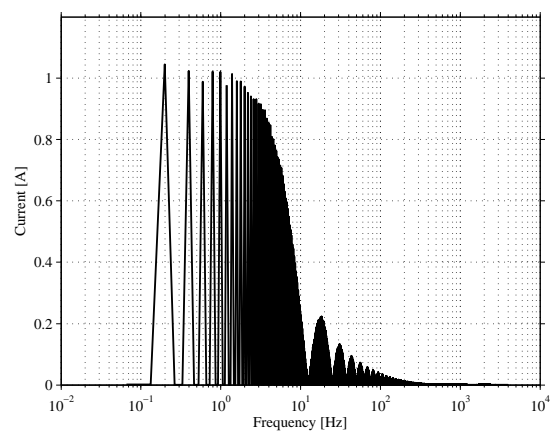


Fig. 6.8 The Fast Fourier Transform (FFT) of the simulated excitation current signal on with battery pack with 2.5 kW power amplitude.

Results of the set-up with high power amplitude

With a power reference with higher amplitude, 4 kW, a higher current in/out of the battery pack can be achieved and accordingly the motor is running in a wider speed range which is between 750 rpm and 3800 rpm, as shown in Fig. 6.9.

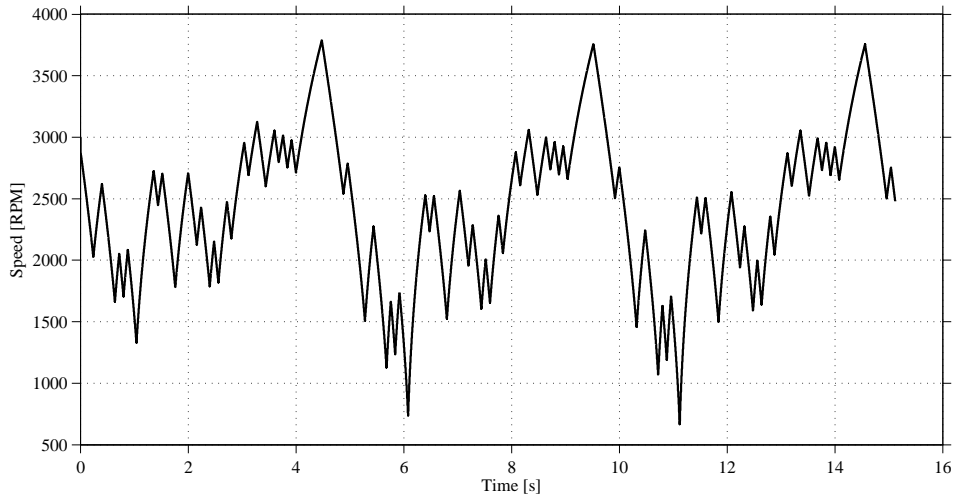


Fig. 6.9 Operation speed range during the simulation with 4 kW power amplitude.

When the motor is running at a high speed, it may operate in field weakening when the stator voltage reaches the battery output voltage. It can be observed according to the stator current in d-axis in Fig. 6.10. The d-axis current is negative when field weakening occurs.

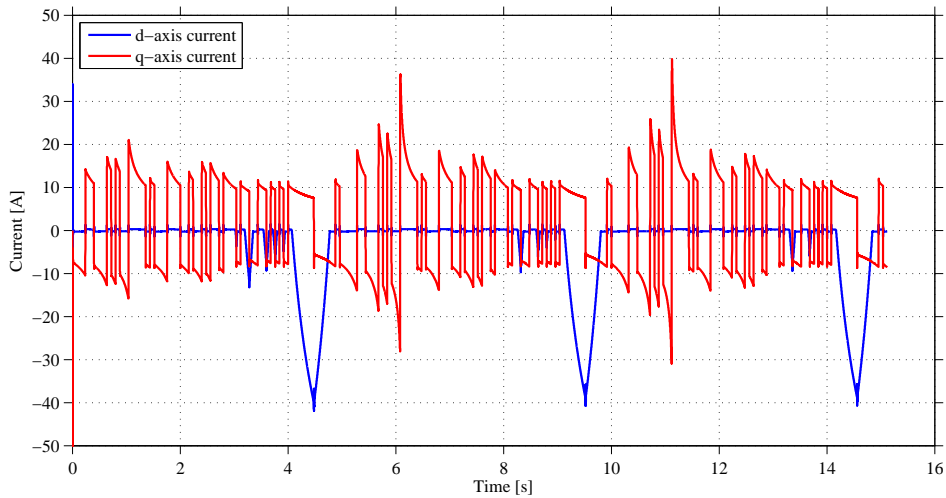


Fig. 6.10 The stator current in d-axis and q-axis during the simulation with 4 kW power amplitude. The d-axis current is negative when field weakening occurs.

The control method with field weakening allows the motor to operate in a wider speed range but on the other hand it introduces more current harmonics in the battery pack current, which can be seen from Fig. 6.11. The battery pack current starts to spread when operating in field weakening.

With more harmonics, the excitation current signal in frequency domain in Fig. 6.12 is a bit distorted compared to the FFT of an ideal PRBS. However, the maximum current amplitude is around 1.7 A which is slightly higher than the previous case but still quite low.

From the simulations on the drive line, it is found that an excitation current signal is possible generate by using the electric motor. This excitation signal is similar to an ideal PRBS and it can be used to identify the battery pack. However, due to the controller bandwidth and the DC-link capacitor, only an excitation signal with a low clock frequency can be generated. The signal with a high clock frequency might be possible to

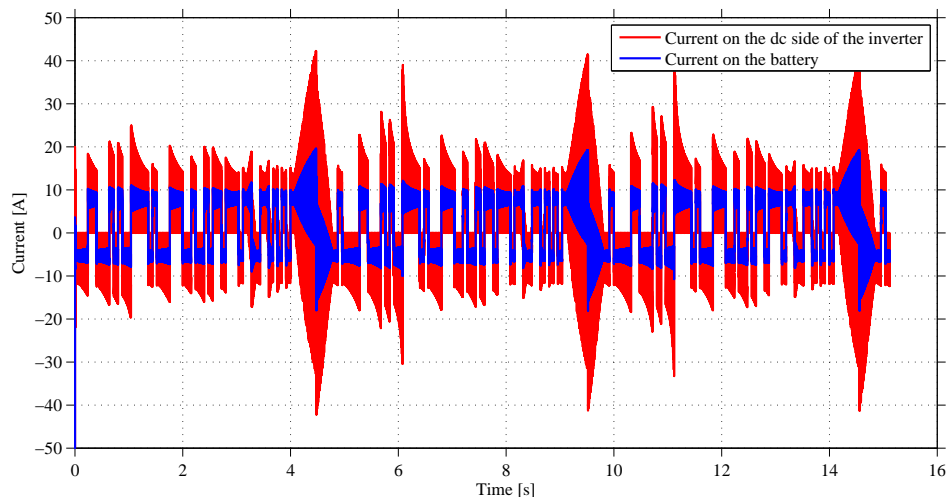


Fig. 6.11 The DC-link current and battery pack current during the simulation with 4 kW power amplitude.

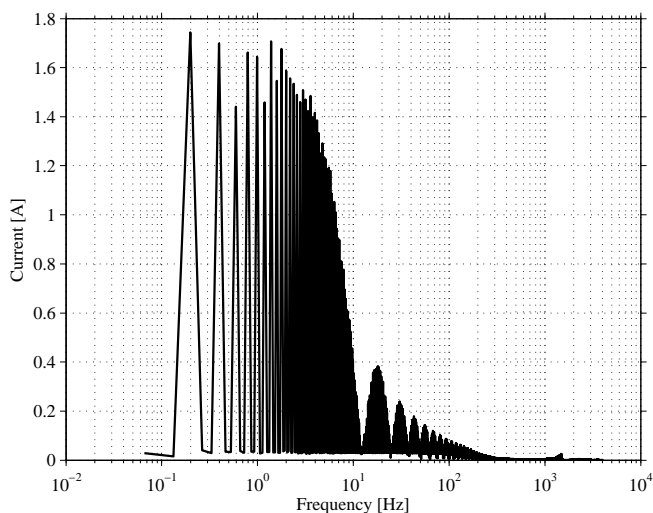


Fig. 6.12 The Fast Fourier Transform (FFT) of the simulated excitation current signal on with battery pack with 4 kW power amplitude.

be generated if the inverter is controlled as a buck converter, which means in this case the motor will be used only as an inductive load. What is more, the currents in both cases are too small to identify a battery pack. This can be improved by adding additional inertia on the motor, for example the transmission and the wheel if the vehicle is lifted.

Both of the battery pack currents in the two cases are applied to a simple battery model like Fig. 2.4. The parameters used in this model are taken from [38] as an example. The EIS of this battery model is shown in Fig. 6.13. The excitation signal with a lower amplitude can give a better result in which case the motor is not operating in field weakening. However, the result will be much worse in reality since the signal to noise ratio (SNR) is very low in the real vehicle applications.

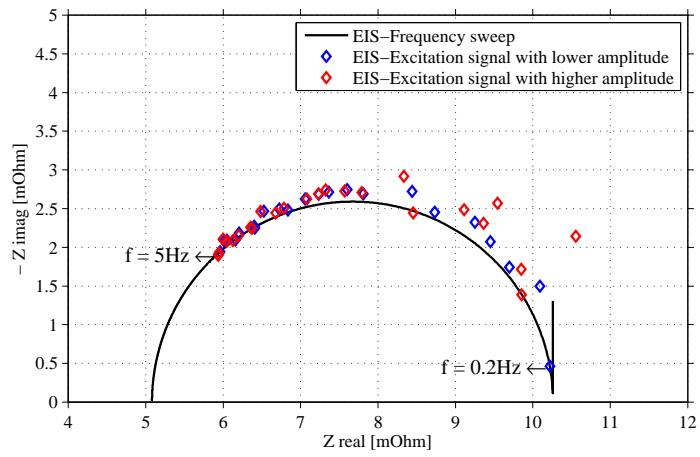


Fig. 6.13 An example of how the excitation signal can be used for system identification. The battery model used is a simplified Randles model and the parameters are taken from an article. The result is better if the motor is not running under field weakening.

Chapter 7

Conclusions and Future Work

In this chapter, the conclusions are presented along with recommendations on how the work could be continued. Further research and investigation are needed to achieve a commercial solution.

7.1 Conclusions

Electrochemical impedance spectroscopy (EIS) of the battery depends on the state of charge (SOC), state of health (SOH), temperature and dynamic state. Therefore, the EIS is an useful tool for the battery diagnostics. This thesis has focused on the method validation of using a pseudo-random binary sequence (PRBS) as the excitation signal to identify the impedance of the battery. The investigation proved that the PRBS can be used to measure the EIS of the battery in a limited frequency range. It can give very similar results to the measurements from a high accuracy impedance analyzer which uses frequency sweep. The PRBS method is valid at different SOC levels and at different temperatures.

The present work also included an analysis about the factors in a PRBS measurement, including the selection of the PRBS bit, current amplitude, sign of the signal, rise time of the current step, cycle number, measurement bandwidth, measurement resolution and sampling frequency. Both experiments and simulations are performed to analyze the above parameters. In the measurements at different SOC levels and temperatures, an 8-bit bipolar PRBS current signal with a 40 Hz clock frequency and 10 A amplitude is used. The PRBS method is stable in a low frequency range, but with a high clock frequency the PRBS method shows a poor result due to the voltage spikes caused by the inductive connections.

The purpose of investigating the PRBS method is to measure the EIS of the battery pack in the electric vehicles/hybrid electric vehicles to improve the battery management unit. A proposal of how to implement the PRBS method is by using the propulsion motor in the drive line as the load to generate an excitation signal like a PRBS. A simulation is performed to show the drive line behavior and the results show that it is possible to some extent to generate an excitation that can be used for the battery impedance identification. However, only an excitation signal with a low clock frequency and low amplitude can be achieved with the current set-up.

7.2 Future work

7.2.1 Improvements for the PRBS method

Due to the low impedance of the battery, the voltage changes caused by the excitation signal are very small compared with the battery rated voltage and they are hard to be measurement accurately. As discussed in the Case set-up, a 16-bit ADC has a higher resolution and it can give a better result than a 12-bit ADC. To increase the resolution even more, one way is to use a higher bit ADC but it will increase the cost. Another way is to use a specially designed operation amplifier. The idea of this amplifier is to remove the DC offset of the signal and only measure the voltage deviations. When designing this amplifier, a stable power source and the isolation need to be taken care of.

During the EIS measurement, a calibration of the measurement equipment can improve the results a lot. More information is discussed in [3]. Other than the PRBS, a multi-sine signal is also a good option for

system identification.

7.2.2 Additional Options for Method Implementation in the Vehicles

During the drive line simulations, it is assumed that the torque rise time is mainly limited by the current controller. However, in reality there is another torque limitation in the automotive application. Detailed information is not available during the thesis.

In the drive line simulation, the DC-link capacitor plays an important role on the performance of the excitation signal. The harmonics are related to the modulation and phase of the motor. It can be seen from the simulations that when the field weakening occurs, more harmonics are introduced to the battery side. It would be interesting to study further on it.

In this thesis, only an excitation signal with a low clock frequency is simulated on the drive line due to the limitation of the current controller. To generate an excitation signal with a higher clock frequency, the inverter can be controlled as a buck converter and motor can be used only as an inductive load. By such an action, it may be possible to have a faster excitation signal on the drive line.

References

- [1] A. Narula, "Modeling of ageing of lithium-ion batteries at low temperatures," Master's thesis, Chalmers University of Technology, 2014.
- [2] J. Groot, "State-of-health estimation of li-ion batteries: Cycle life test methods," *Chalmers University of Technology, Göteborg*, 2012.
- [3] D. Howey, P. D. Mitcheson, V. Yufit, G. J. Offer, N. P. Brandon *et al.*, "Online measurement of battery impedance using motor controller excitation," *Vehicular Technology, IEEE Transactions on*, vol. 63, no. 6, pp. 2557–2566, 2014.
- [4] P. Fundaro, "Impedance trac based fuel gauging," Texas Instruments, Tech. Rep., 2007.
- [5] S. Miller and D. Childers, *Probability and random processes: With applications to signal processing and communications*. Academic Press, 2012.
- [6] T. Roinila, M. Vilkkko, and J. Sun, "Online grid impedance measurement using discrete-interval binary sequence injection," *Emerging and Selected Topics in Power Electronics, IEEE Journal of*, vol. 2, no. 4, pp. 985–993, 2014.
- [7] A. Fairweather, M. Foster, and D. Stone, "Battery parameter identification with pseudo random binary sequence excitation (prbs)," *Journal of Power Sources*, vol. 196, no. 22, pp. 9398–9406, 2011.
- [8] R. Al Nazer, V. Cattin, P. Granjon, M. Montaru, and M. Ranieri, "Broadband identification of battery electrical impedance for hevs," *Vehicular Technology, IEEE Transactions on*, vol. 62, no. 7, pp. 2896–2905, 2013.
- [9] R. Robinson, "System noise as a signal source for impedance measurements on battery strings," in *Telecommunications Energy Conference, INTELEC'93. 15th International*, vol. 2. IEEE, 1993, pp. 365–368.
- [10] J. Remmlinger, M. Buchholz, M. Meiler, P. Bernreuter, and K. Dietmayer, "State-of-health monitoring of lithium-ion batteries in electric vehicles by on-board internal resistance estimation," *Journal of Power Sources*, vol. 196, no. 12, pp. 5357–5363, 2011.
- [11] O. Bohlen, S. Buller, R. W. De Doncker, M. Gelbke, and R. Naumann, "Impedance based battery diagnosis for automotive applications," in *Power Electronics Specialists Conference, 2004. PESC 04. 2004 IEEE 35th Annual*, vol. 4. IEEE, 2004, pp. 2792–2797.
- [12] D. V. Do, C. Forgez, K. El Kadri Benkara, and G. Friedrich, "Impedance observer for a li-ion battery using kalman filter," *Vehicular Technology, IEEE Transactions on*, vol. 58, no. 8, pp. 3930–3937, 2009.
- [13] M. Montaru and S. Pelissier, "Frequency and temporal identification of a li-ion polymer battery model using fractional impedance," *Oil & Gas Science and Technology–Revue de l'Institut Français du Pétrole*, vol. 65, no. 1, pp. 67–78, 2010.
- [14] E. Kuhn, C. Forgez, P. Lagonotte, and G. Friedrich, "Modelling ni-mh battery using cauer and foster structures," *Journal of power sources*, vol. 158, no. 2, pp. 1490–1497, 2006.
- [15] F. A. E., C. K. Jr., and A. Kusko, *Electric Machinery*. McGraw-Hill, 1971.

- [16] *The Authoritative Dictionary of IEEE Standards Terms, Seventh Edition.* IEEE Press.
- [17] F. Renken, "Analytic calculation of the dc-link capacitor current for pulsed three-phase inverters," in *Proc. 11th Int. Conf. Power Electron. Motion Control*, 2004.
- [18] *Siemens CL75 user manual.*
- [19] A. Fuhs, *Hybrid Vehicles: and the Future of Personal Transportation.* CRC Press, 2008.
- [20] C. J. Kimble and S. W. Steele, "Series-parallel battery array conversion," Aug. 6 2002, uS Patent 6,430,692.
- [21] M. E. Orazem and B. Tribollet, *Electrochemical impedance spectroscopy.* John Wiley & Sons, 2011, vol. 48.
- [22] J. R. Macdonald and E. Barsoukov, "Impedance spectroscopy: theory, experiment, and applications," *History*, vol. 1, p. 8, 2005.
- [23] H. v. Helmholtz, "Ueber einige gesetze der vertheilung elektrischer ströme in körperlichen leitern, mit anwendung auf die thierisch-elektrischen versuche (schluss.)," *Annalen der Physik*, vol. 165, no. 7, pp. 353–377, 1853.
- [24] Y. Barsoukov and J. Qian, *Battery power management for portable devices.* Artech House, 2013.
- [25] J. Shuttleworth, "Battery monitoring unit," *SAE International, Automotive Engineering Magazine*, 2010.
- [26] A. C. Fischer-Cripps, *The Electronics Companion: Devices and Circuits for Physicists and Engineers.* CRC Press, 2014.
- [27] A. Millner, "Modeling lithium ion battery degradation in electric vehicles," in *Innovative Technologies for an Efficient and Reliable Electricity Supply (CITRES), 2010 IEEE Conference on.* IEEE, 2010, pp. 349–356.
- [28] O. Heaviside, "The electrician," *23rd July*, p. 212, 1886.
- [29] S. M. Rezvanizani, Z. Liu, Y. Chen, and J. Lee, "Review and recent advances in battery health monitoring and prognostics technologies for electric vehicle (ev) safety and mobility," *Journal of Power Sources*, vol. 256, pp. 110–124, 2014.
- [30] M. Shahriari and M. Farrokhi, "State of health estimation of vrla batteries using fuzzy logic," in *Electrical Engineering (ICEE), 2010 18th Iranian Conference on.* IEEE, 2010, pp. 629–634.
- [31] H. Okawara, "Dsp-based testing fundamentals 50: Prbs (pseudorandom binary sequence)," *Verigy's Go/Semi Newsletter*, 2008.
- [32] J. N. Davidson, D. Stone, M. P. Foster, D. T. Gladwin *et al.*, "Improved bandwidth and noise resilience in thermal impedance spectroscopy by mixing prbs signals," *Power Electronics, IEEE Transactions on*, vol. 29, no. 9, pp. 4817–4828, 2014.
- [33] A. Jossen, "Fundamentals of battery dynamics," *Journal of Power Sources*, vol. 154, no. 2, pp. 530–538, 2006.
- [34] K. J. Aström and R. M. Murray, *Feedback systems: an introduction for scientists and engineers.* Princeton university press, 2010.
- [35] T. Wescott, "Sampling: What nyquist didn't say, and what to do about it," Wescott Design Services, Tech. Rep., 2015.
- [36] R. Krishnan, *Permanent magnet synchronous and brushless DC motor drives.* CRC press, 2009.
- [37] L. Harnefors and H.-P. Nee, "Control of variable-speed drives," *Course compendium, Malardalen University, Sweden*, 2002.
- [38] A. Fairweather, M. Foster, and D. Stone, "Battery parameter identification with pseudo random binary sequence excitation (prbs)," *Journal of Power Sources*, vol. 196, no. 22, pp. 9398–9406, 2011.

Appendix A

Test Conditions

A.1 Battery Cell Specification



Fig. A.1 LG Chem 41 Ah battery.

Table A.1: Battery cell specification.

Application	EV / PHEV
Shape	Prismatic type (soft-pack) : Al laminated pouch
Chemical characteristics	Mn/NMC cathode, Carbon/Graphite anode
Nominal capacity (0.5C)	41 Ah
Nominal voltage (0.5C)	3.75 V
Voltage range (Continuous)	3.0 V to 4.15 V
Energy density	159 Wh/kg
Power density	2000 W/kg (10sec @ SOC50)

A.2 Layout of the Experiment Set-up

The hardware set-up in the lab is shown in Fig. A.2, A.3 and A.4. The schematic of the setup is summarized in Fig. A.5.

A set-up of the GAMRY involves a 4-wire measurement to increase the accuracy. To reduce the disturbances, the power cable and signal cable need to be kept as far away as possible. Cables which carry the same signal with opposite direction need to be twisted, as shown in Fig. A.4.

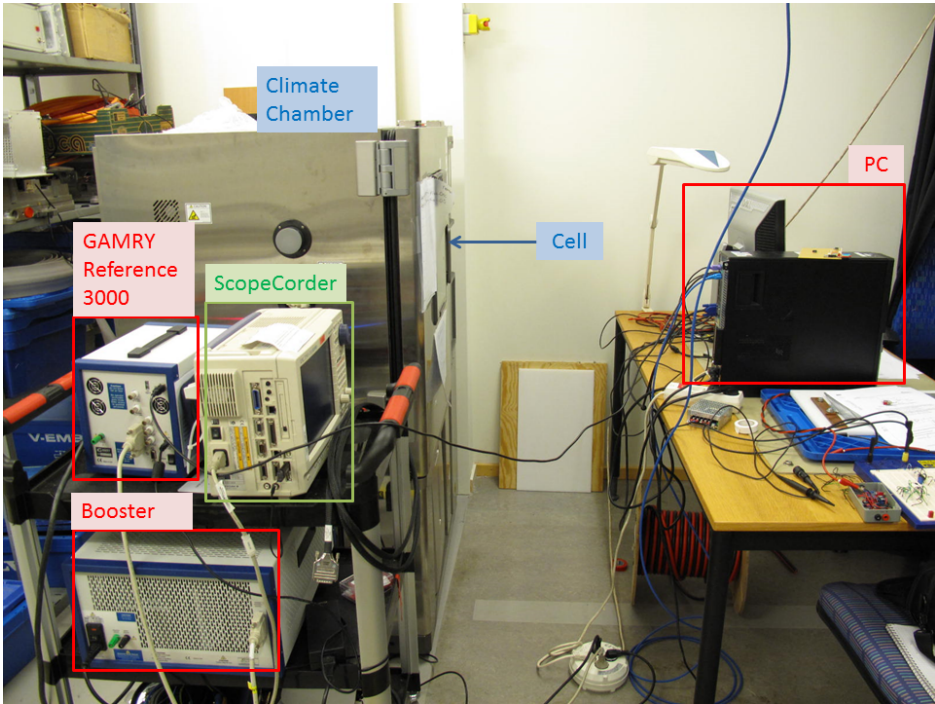


Fig. A.2 Hardware set-up in the lab during the experimental phase of PRBS method validation. The battery cell is in the climate chamber with a controlled temperature. The GAMRY Reference 3000, the Booster and the Scopecorder are used for the PRBS generation and measurement.



Fig. A.3 Current Probe Model PR30 used to measure the current during the experiments. It is a high bandwidth DC/AC current probe.

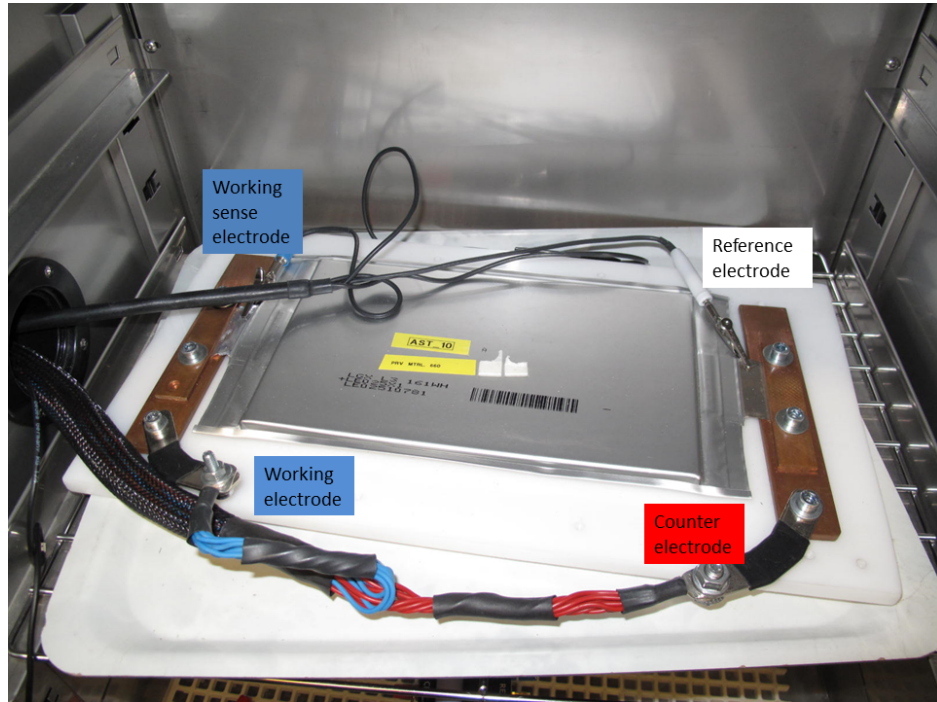


Fig. A.4 The 4-wire connection on the cell to increase the measurement accuracy (inside the climate chamber).

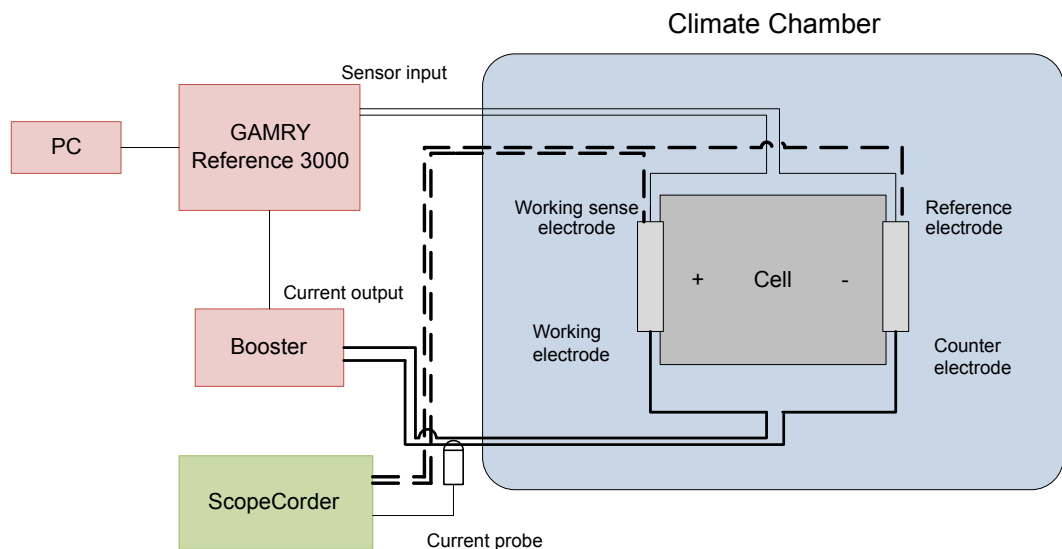


Fig. A.5 Layout of the experiments set-up showing the connection of the PRBS generator and measurement with the battery cell. The 4-wire connection is used.

Appendix B

Simulation Matrix

Number of experiment:	Amplitude	SOC	SOH	Temperature	Switch Frequency	Cycle Time	PRBS Bits	Sample Time
1 (Standard)	10	60	100	20	10	5	8	0.001
2	0.1	60	100	20	10	5	8	0.001
3	1	60	100	20	10	5	8	0.001
4	50	60	100	20	10	5	8	0.001
5	100	60	100	20	10	5	8	0.001
6	10	0	100	20	10	5	8	0.001
7	10	20	100	20	10	5	8	0.001
8	10	40	100	20	10	5	8	0.001
9	10	80	100	20	10	5	8	0.001
10	10	100	100	20	10	5	8	0.001
11	10	60	0	20	10	5	8	0.001
12	10	60	30	20	10	5	8	0.001
13	10	60	60	20	10	5	8	0.001
14	10	60	100	-20	10	5	8	0.001
15	10	60	100	0	10	5	8	0.001
16	10	60	100	35	10	5	8	0.001
17	10	60	100	20	20	5	8	0.001
18	10	60	100	20	40	5	8	0.001
19	10	60	100	20	60	5	8	0.001
20	10	60	100	20	100	5	8	0.001
21	10	60	100	20	10	10	8	0.001
22	10	60	100	20	10	20	8	0.001
23	10	60	100	20	10	3	8	0.001
24	10	60	100	20	10	1	8	0.001
25	10	60	100	20	10	5	6	0.001
26	10	60	100	20	10	5	10	0.001
27	10	60	100	20	10	5	12	0.001
28	10	60	100	20	10	5	14	0.001
29	10	60	100	20	10	5	8	0.1
30	10	60	100	20	10	5	8	0.00001

Fig. B.1 Table of simulations for the validation of the PRBS method implementation